ZnO BASED PHOTO-THIN-FILM-TRANSISTORS WITH ACTIVELY TUNABLE PHOTORESPONSE IN THE VISIBLE SPECTRUM

A THESIS
SUBMITTED TO THE DEPARTMENT OF ELECTRICAL AND ELECTRONICS ENGINEERING
AND THE GRADUATE SCHOOL OF ENGINEERING AND SCIENCE
OF BILKENT UNIVERSITY
IN PARTIAL FULFILLMENT OF THE REQUIREMENTS
FOR THE DEGREE OF
MASTER OF SCIENCE

By
Levent Erdal Aygün
August 2013

I certify that I have read this thesis and that in my opinion it is fully adequate, in scope and in quality, as a thesis for the degree of Master of Science.

____

Assist. Prof. Dr. Ali Kemal Okyay (Supervisor)

I certify that I have read this thesis and that in my opinion it is fully adequate, in scope and in quality, as a thesis for the degree of Master of Science.

____

Assoc. Prof. Dr. Mehmet Bayındır

I certify that I have read this thesis and that in my opinion it is fully adequate, in scope and in quality, as a thesis for the degree of Master of Science.

____

Assist. Prof. Dr. Necmi Bıyıklı

Approved for the Graduate School of Engineering and Science:

____

Prof. Dr. Levent Onural

Director of Graduate School

ABSTRACT

ZnO BASED PHOTO-THIN-FILM-TRANSISTORS WITH ACTIVELY TUNABLE PHOTORESPONSE IN THE VISIBLE SPECTRUM

Levent Erdal Aygün

M.S. in Electrical and Electronics Engineering

Supervisor: Assist. Prof. Dr. Ali Kemal Okyay

August 2013

Zinc oxide, ZnO, is an important material for wide range of optoelectronic device applications. Especially, ZnO is famous with its large exciton binding energy of 60 meV which makes it a good candidate for ultraviolet light emitting diodes and lasers. Moreover, its high carrier mobility and wide band gap of 3.37 eV (368 nm) makes it a promising material for transparent electronics and UV photodetectors. However, ZnO has crystallographic defect states (e.g. oxygen vacancies, zinc interstitials) which degrade the performance of ZnO based LEDs, lasers and UV photodiodes.

In this thesis, ZnO based photo-thin-film-transistors (photo-TFTs) with visible light response by using their defect states to absorb subbandgap photons are investigated. The design, fabrication and characterization of ZnO based photo-TFTs are presented. A photo-TFT is a three-terminal optoelectronic device that is a photoconductor structure with an additional gate terminal which actively tunes electrical and optical properties of photoconductive material.

In a clean room environment, ZnO based photo-TFTs with various device sizes are fabricated at different ZnO channel layer deposition temperatures (ranging from 80 to 250 °C). Initially, TFT characteristics of fabricated devices are

characterized to show that the gate terminal dynamically modulates ZnO's channel conductivity. Moreover, the effects of the device size and the deposition temperature on device performance are investigated. Then, the optical characterization of ZnO film deposited at 250° C is conducted via absorption and photoluminescence measurements in order to investigate its visible light absorption characteristics and the energy levels of its defect states in the forbidden band gap of ZnO. After that, the responsivity measurements are reported from ZnO based photo-TFTs fabricated at 250 °C and the active tuning mechanism of visible light photoresponse is discussed. Finally, the effects of the deposition temperature and the device size on the visible light responsivity are presented.

Keywords: ZnO, TFT, photoconductor, photo-TFT, photodetector,

ÖZET

GÖRÜNÜR IŞIĞA TEPKİSİ AKTİF OLARAK AYARLANABİLEN ZnO BAZLI FOTO-İNCE-FİLM-TRANSİSTÖRLER

Levent Erdal Aygün

Elektrik ve Elektronik Mühendisliği Bölümü Yüksek Lisans

Tez Yöneticisi: Yar. Doç. Prof. Dr. Ali Kemal Okyay

Ağustos 2013

Çinko oksit, ZnO, birçok optoelektronik cihaz uygulaması için önemli bir malzemedir. Özellikle yüksek eksiton bağlanma enerjisi (60 meV) ile ünlü bir malzemedir. Bu yüksek bağlanma enerjisi onu morötesi ışık-yayan-diyotlar (LEDs) ve lazerler için iyi bir aday malzeme yapar. Yüksek elektriksel taşıyıcı hareketliliği ve geniş enerji bant aralığı (3.37 eV – 368 nm) sayesinde saydam elektronik aygıtlar ve morötesi ışık sensörlerinde kullanılmak için aday bir malzemedir. Fakat ZnO kristal yapısı içerisinde hata seviyelerine sahiptir (örneğin eksik oksijen ya da fazla çinko atomu). Bu kristal hataları ZnO bazlı morötesi LED, lazer ve ışık sensörlerinin performanslarını düşürmektedir.

Bu tez çalışmasında, kristal hatalarını kullanarak band aralığından daha düşük enerjili fotonları emen ve görünür ışığa tepki veren ZnO bazlı foto-ince-film-transistörler (photo-TFT) incelendi. ZnO bazlı foto-ince-film-transistörlerin dizayn, üretim ve karakterizasyonu sunuldu. Üç kutuplu optoelektronik bir cihaz olan photo-TFT'nin yapısı basit olarak iki kutuplu ve ışıkla iletkenliği değişen bir yarı iletkene üçüncü bir kutup eklenmiş halidir. Bu üçüncü kutup (kapı kutbu) yarı iletkenin elektriksel ve optik özelliklerini aktif olarak kontrol eder.

Temiz oda ortamlarında, çeşitli boylarda ve kaplama sıcaklıklarında ZnO bazlı photo-TFT'ler üretilmiştir. İlk olarak, üretilen aygıtların transistör

karakterizasyonu yapılarak, kapı kutbunun ZnO'ın elektriksel özelliklerini dinamik olarak kontrol edebildiği gösterildi. Aygıt boyutunun ve kaplama sıcaklığının cihaz performansı üzerine etkileri incelendi. 250 °C'de kaplanmış ZnO katmanının emilim ve ışıma karakterizasyonu yapılarak, görünür ışığı absorb etme yeteneği ve hata seviyelerinin ZnO'ın enerji bant aralığındaki enerji seviyeleri araştırıldı. Sonrasında, 250 °C kaplanmış ZnO bazlı photo-TFT'lerin ışığa verdikleri elektriksel tepki (responsivity) ölçülerek aktif olarak ayarlanabilen görünür ışığa tepki mekanizması tartışıldı. Son olarak, ZnO kaplama sıcaklığının ve aygıt boyutunun cihaz performansı üzerine etkileri sunuldu.

Anahtar sözcükler: ZnO, TFT, foto-iletken, photo-TFT, ışık detektörü

To my family and friends…

Acknowledgements

I would like to express my sincere gratitude to Asst. Prof. Dr. Ali Kemal Okyay for his attention, support, and invaluable guidance throughout my study, as well as for his patience and insight. He let me be in the driver's seat regarding my M.S. research and provided great freedom to develop my research skills and collaborate in various projects. I am grateful for having the chance to work with him.

I am indebted to my dissertation committee, Assoc. Prof. Dr. Mehmet Bayındır and Asst. Prof. Dr. Necmi Bıyıklı for accepting to read and review this thesis and for their suggestions.

I am also thankful to the Department of Electrical and Electronics Engineering of Bilkent University and UNAM-Institute of Materials Science and Nanotechnology for creating a challenging environment. I would also like to acknowledge the financial support that I received from TUBİTAK BİDEB 2210 Program.

I have been blessed with a friendly and cheerful group of fellow students. I am especially grateful to Feyza Bozkurt Oruc and Fatih Bilge Atar who thought me everything that I know about clean room fabrication processes and characterization setups. I would like to thank my past and present lab mates in Okyay Team: Burak Tekcan, Enes Battal, Sami Bolat, Temmuz Ceyhan, Furkan Cimen, Muhammad Maiz Ghauri, Amir Ghobadi, Abdullah Gulle, Oguz Hanoglu, Yunus Emre Kesim, Ali Cahit Kosger, Amin Nazirzadeh, Ayse Ozcan, Elif Ozgoztasi, Kazim Gurkan Polat, Ferhat Tasdemir, Gamze Ulusoy, Alper Yesilyurt, Taha Alper Yogurt, Dr. Hakan Karaagac and Dr. Sabri Alkis.

I would like to appreciate supports coming from the UNAM family: Inci(k) Donmez, Deniz Kocaay, Alican Noyan, Dr. Asli Noyan, Engin Cagatay, Cagla Ozgit, Pelin Kubra Isgor, Adem Sarac, Koray Mizrak, Ruslan Garifullin, Dr. Mehmet Solmaz and Dr. Handan Acar. We really had a good time in UNAM and I cherish those moments.

I would like send my special thanks to dear friends Ahmet Cinar, Fethi Burak Sazoglu, Ahmet Yukselturk, Seyma Canik for their everlasting support during my study. I would like to also thank Burcin Cakir for encouraging me to apply Princeton; Cetin Sahin for being the best roommate during my undergraduate years and being the best host at UCSB; Alexandra Zehra Aksu for being the role model as a good person; Cansu Yazganarıkan and Caner Mercan for being so nice to me.

To those not mentioned here, I am no less thankful but it would be impossible to mention all of your contributions.

There are no words in the dictionary to express my deepest sense of gratitude to my parents and my brother. Without their support, I could not finish this adventure.

Contents

Acknowledgement……..……………..……………………………...viii
List of Figures …..……………………………..……………….....xii
List of Tables…..……………………………………………...……xvi
Chapter 1 Introduction 1
1.1 Material properties and device applications of zinc oxide 1
1.2 Motivation 3
1.3 Organization of the thesis 4
Chapter 2 Scientific Background 6
2.1 Transistor basics 6
2.1.1 MOSFET operation 7
2.1.2 Ideal current-voltage relations for n-channel MOSFET ... 9
2.1.3 Thin Film Transistors 10
2.2 Semiconductor Photodetectors 12
2.2.1 Photoconductors 13
2.2.2 Photoconduction and photoconductive gain 14
2.2.3 Photo-Thin-Film-Transistor.. 16
2.3 Defect characteristics of ZnO 17
2.3.1 Violet - blue emission:.. 17
2.3.2 Green emission: 19
2.3.3 Orange-red emission:... 19
Chapter 3 Experimental Methods.. 20
3.1 Device Fabrication 20
3.1.1 Surface preparation 20
3.1.2 Formation of the isolation layer.................................... 21
3.1.3 Formation of the gate stack... 22
3.1.4 Formation of the electrical contacts............................... 24
3.2 Characterization methods 25
3.2.1 Photoluminescence measurements 25

3.2.2 Spectral photoresponsivity measurements 27
Chapter 4 Results and Discussions 31
4.1 Transistor characteristics 31
4.2 Defect state analysis 36
4.3 Actively tunable photoresponse in the visible spectrum 40
4.4 Effects of the device size on photoresponse to visible light....... 42
4.5 Effects of deposition temperature of channel layer on the photoresponsivity 45
Chapter 5 Conclusions 47
Bibliography ……………………………..………………………………51

List of Figures

Figure 1.1: A quartz substrate with a 40-nm-thick ZnO film is placed over UNAM logo. The film is transparent under the visible light. 2

Figure 1.2: Full color AMOLED display [23] 2

Figure 2.1: A n-channel enhancement mode MOSFET: a) cross section of its structure, b) equivalent circuit in off state , c) Energy-band diagram without bias d) I_D-V_G relation with increasing gate voltage where green line separates saturation and non-saturation regions.. 8

Figure 2.2: Cross sections of n-channel enhancement mode MOSFET for the operation modes of a) off, b) non-saturation, c) transition between nonsaturation and saturation, d) saturation. 10

Figure 2.3: A bottom-gate-top-contact TFT architecture, used in this study. 11

Figure 2.4: Photodetection process in the semiconductor photodetectors: (i) absorption of incident photon, (ii) separation and drift of electron-hole pair and collection of drifted charge carriers.. 12

Figure 2.5: Photoexcitation mechanisms: (i) from valence band to conduction band, (ii) from valence band to defect state, and (iii) from defect state to conduction band. 13

Figure 2.6: Energy band diagram that shows the energy levels of crystallographic defects of ZnO reported in the literature. 18

Figure 3.1: In order to reduce leakage between gate and top contacts, 200-nm-thick SiO_2 layer is deposited (a) and patterned (b) to define active regions 22

Figure 3.2: Deposition of gate oxide and channel layers. a) 20 nm thick Al_2O_3 and b) 14 nm thick ZnO deposited using ALD technique. c) The deposited ZnO layer is patterned with lithography and diluted H_2SO_4 wet etch solution. 24

Figure 3.3: 100 nm thick Al layer deposited and patterned using lift-off technique to form source and drain contacts. a) Schematic of a finalized TFT design. b) A microscope image taken from a sample after the lithography step which defines source and drain contact regions. 25

Figure 3.4: Schematic of a typical photoluminescence measurement setup 26

Figure 3.5: Responsivity measurement setup. Monochrome light is focused on the fabricated device from the top at normal incidence. The photocurrent between drain and source terminals is measured with a lock-in amplifier. 28

Figure 3.6: Incident optical power measured by calibrated Si photodetector with and without a long pass filter at 500 nm. 29

Figure 3.7: Incident optical power measured by calibrated Si photodetector without a long pass filter at 500 nm. 30

Figure 4.1: I_D-V_G characteristics of ZnO-based TFTs which indicate n-channel enhancement mode transistor characteristics. The device also has a threshold voltage of 3.79 V and a decent on/off ratio of 10^9. The channel layer of measured device is deposited at 80°C and its both channel length and width are 100 μm. 1 V of drain bias is applied. 32

Figure 4.2: I_D-V_G characteristics of devices, having various channel sizes, are shown in (a) logarithmic and (b) linear scale. The sizes shown in the legends are channel width and channel length, respectively. Measurements are taken from devices with a channel layer deposited at 80 °C and 1 V is applied as the drain to source bias. 33

Figure 4.3: Scaling behavior of ZnO based TFTs fabricated at 80 °C. All devices are biased with 1 V drain bias and 8 V gate bias. The dashed red line shows linear drain current scaling characteristics of fabricated TFTs. 34

Figure 4.4: I_D-V_G characteristics of devices having ZnO channel deposited at various temperatures... 34

Figure 4.5: Threshold voltage calculation using extrapolation in the saturation region technique. $I_D^{0.5}$-V_G characteristics of devices are plotted and drain current values are linearly extrapolated to zero drain current value............................. 35

Figure 4.6: Spectral photoluminescence of ZnO layer coated on quartz substrate. Photoluminescence intensity is given in arbitrary units. Photoluminescence excitation wavelength is 290 nm. 37

Figure 4.7: Energy level of trap states. Two possible trap-assisted emission routes: Route I: trap energy states are closer to the valence band. Conduction band electrons and localized holes of trap states (unoccupied trap) recombine and emit light (1). Route II: Trap energy states are closer to the conduction band. Localized electrons of trap states (occupied trap) and free holes of valence band recombine and emit light (2). 38

Figure 4.8: Measured photoluminescence intensity at 510 nm (2.43 eV) for various excitation wavelengths. The dashed line shows the bandgap energy of ZnO.. 38

Figure 4.9: Absorption spectrum of ZnO layer on a quartz substrate. Absorption is given in arbitrary units. The dashed line shows the bandgap energy of ZnO. 39

Figure 4.10: Absorption mechanisms of ZnO: Interband (1), valence band to trap state (2), and trap state to conduction band (3). 40

Figure 4.11: Spectral responsivity of a ZnO based TFT at 250 °C with a device size 200 µm x 200 µm and under a drain bias of 3 V....................................... 41

Figure 4.12: Spectral responsivity of a ZnO based TFT at 250 °C for various device sizes while constant V_D bias of 3 V is applied. Corresponding device channel lengths and widths are a) 50 μm - 50 μm, b) 100 μm - 100 μm, c) 150 μm - 150 μm, d) 200 μm - 200 μm, e) 150 μm - 100 μm. 43

Figure 4.13: Responsivity per the square of channel length is plotted for ZnO based photo-TFTs at 250 °C. Constant V_D and V_G of -3 and 3 V are applied respectively. Legends show channel length and width respectively. 44

Figure 4.14: Spectral responsivity of ZnO based TFTs with a channel layer deposited at a) 250 °C, b) 200 °C, c) 120 °C, d) 100 °C, e) 80 °C. The device size is kept constant as 200 μm to 200 μm and 3 V drain bias is applied. 45

Figure 4.15: Deposition temperature dependent responsivity of ZnO based TFTs at λ = 550nm. The device size, V_G and V_D are chosen as 200 μm to 200 μm, -3 V and 3 V, respectively. 46

List of Tables

Table 3.1: ALD recipes for depositing ZnO at various temperatures 23

Table 4.1: Fundamental transistor characteristics of ZnO based TFTs.............. 36

Chapter 1

Introduction

1.1 Material properties and device applications of zinc oxide

Zinc oxide has drawn a great deal of interest in recent years, owing to its exciting material properties such as large exciton binding energy, high carrier mobility and wide band gap. ZnO has an exciton binding energy of 60 meV which is larger than the room temperature thermal energy (26 meV) and the exciton binding energies of other III-V and II-VI widebandgap semiconductors such as GaN (25 meV) and ZnSe (20 meV) [1, 2]. Having large exciton binding energy makes ZnO a promising candidate for ultraviolet light emitting diodes and lasers [3-10].

ZnO is also attracting interest as an alternative to amorphous Si (a-Si) in thin-film transistors (TFTs) especially in modern display applications [11]. ZnO-based TFTs have higher reported carrier mobilities than a-Si-based TFTs [12]. ZnO is transparent under the visible light (See Figure 1.1) because of its large

band gap and it is becoming the leading material of choice in transparent TFTs (TTFTs) [13-19]. Recently, TTFTs have emerging applications such as active-matrix organic light-emitting diodes (AMOLEDs) [11, 18, 20, 21] (See Figure 1.2) and active-matrix liquid crystal displays (AM-LCDs) [11, 22]. ZnO channel layer is obtained using a wide range of deposition techniques such as pulsed laser deposition [13], ion beam sputtering [14], RF magnetron sputtering [15], metal-organic chemical vapor deposition [16], and atomic layer deposition (ALD) [17, 18].

Figure 1.1: A quartz substrate with a 40-nm-thick ZnO film is placed over UNAM logo. The film is transparent under the visible light.

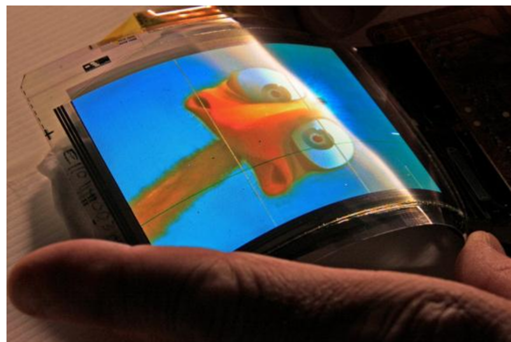

Figure 1.2: Full color AMOLED display [23]

As a direct and wide band gap semiconductor (E_g = 3.37 eV), ZnO is also used to detect photons in the ultraviolet (UV) regime [24]. Such UV photodetectors have wide range of applications such as satellite based missile plume detection, solar astronomy, air pollution monitoring and high temperature flame detection [25-29]. ZnO is a naturally n-type doped semiconductor due to its

crystallographic defects [24]. Although there are some reports on p-type ZnO films, it is difficult to achieve a reliable p-type ZnO to make p-n or p-i-n type photodiodes [7, 30-35]. Therefore, metal-semiconductor-metal (MSM) structure is commonly used to design ZnO based UV photodetectors and such devices worked as either Schottky photodiode or photoconductors depending on contact metal selection. UV light photoresponsivity values as high as 400 A/W are reported in the literature for the photodetectors having ZnO layers, which are deposited with metalorganic chemical vapor deposition (MOCVD) technique [25]. Moreover, UV photodetectors with ZnO nanowires are also investigated in the literature in order to improve collection efficiency from ZnO [36-38].

Its crystallographic defects make ZnO an even more interesting material. When ZnO is optically or electrically excited, it emits light in a broad spectrum through these defect centers. The presence of these defects degrades the performance of UV LEDs, lasers and photodiodes. Therefore, there is an ongoing research that aims to understand and eliminate the causes of these defects [1, 39, 40]. On the other hand, these defects significantly improve the performance of photoconductors by providing trap states and photoconductive gain [37].

1.2 Motivation

ZnO based UV photoconductors with internal gains as high as 10^8 are already reported in the literature [37]. However, these devices suffer from slow rise and fall times due to trap related mechanisms. In order to solve this problem, Jeon et. al. proposed gated three terminal device architecture to improve the speed of photoconductors [41]. The suggested architecture has an additional gate terminal to reset the conductivity of photoconductive layer, indium zinc oxide (IZO) in case of Jeon's work. This layer has defects to trap holes and provide photoconductive gain. However, when the light exposure stops, it takes long

time to return to its initial dark state. This time period is reduced by applying external gate bias in order to reset the device. When the proposed device is biased into accumulation region by the gate terminal, electrons are attracted to the IZO layer and trapped holes quickly recombine with the accumulation electrons. This resetting process returns the device to its initial state and prepares it for the next measurement cycle.

Our motivation in this study is to investigate visible light photodetection properties of ZnO layer and design ZnO based photo-TFT that have actively tunable photoresponse in the visible region. Such a device can be used as transparent visible light photodetector or as a smart glass that has electrically tunable transparency.

1.3 Organization of the thesis

This thesis reports the design, fabrication and characterization of a three-terminal optoelectronic device, a photo-TFT, which has actively tunable response to visible light.

Chapter 2 provides a required fundamental scientific background to understand the electrical and optical properties of such devices. The proposed device is a combination of TFT and photoconductor. Therefore, the basic operation principles of these devices are reviewed, separately. Then, a brief overview of sub-band gap emission mechanisms of ZnO is provided with corresponding defect state related transitions.

Chapter 3 gives a detailed recipe for the fabrication steps of ZnO based photo-TFTs and explains characterization methods that are used to analyze the device performance.

Chapter 4 presents the electrical and optical characterization results of fabricated devices and discusses the underlying physical mechanisms that enable active tuning of the visible light photoresponse of ZnO based photo-TFTs. Moreover, the effects of the deposition temperature of ZnO layer and the device size on the performance of ZnO based photo-TFTs are analyzed.

Chapter 5 concludes the thesis with a summary of the work done for this study and the future directions based on the findings in this thesis.

Chapter 2

Scientific Background

2.1 Transistor basics

A transistor is a three-terminal device where the current between two terminals can be controlled by the voltage (or current) bias applied at the third terminal. Transistors can be separated as bipolar junction transistors (BJTs) and field effect transistors (FETs). The BJT is operated by the injection and collection of minority carriers from the third terminal, namely the base. Therefore such devices are called as bipolar since both electrons and holes play important roles. On the other hand, the FET is a majority carrier device, so it is called as a unipolar transistor. Also, the current between two terminals of FET is controlled by the voltage bias applied from the third terminal, namely the gate.

There are several types of FETs depending on how the width of depletion region is modulated. The junction-FET (JFET) is a transistor in which the gate bias controls depletion width of a reverse p-n junction. In metal-semiconductor-FET (MESFET) and metal-insulator-semiconductor FET (MISFET), the gate controls

the depletion width of a Schottky junction, but MISFET has an additional insulator layer between the metal and semiconductor to reduce the gate leakage. The metal-oxide-semiconductor FET (MOSFET) is a MISFET that has an oxide layer as the insulator.

Transistors are mainly used for two operations, amplification and switching. The amplification could be achieved by applying a small AC signal to the third terminal in order to generate a larger signal between other two terminals. The switching operation is basically moving a transistor between its on (current passing) and off (current blocked) states.

2.1.1 MOSFET operation

A typical n-channel enhancement mode MOSFET structure is shown in Figure 2.1 (a). The highly n-type doped (n+) regions are the source and drain terminals. The thin oxide layer isolates the channel region from the gate metal and reduces leakage from the gate. The top metal layers are used to apply voltage bias from the gate terminal and to get electrical contact to the source and drain regions.

Without an external gate bias there is no current flow between source and drain regions since the FET structure has the formation of two back-to-back p-n diodes as shown in Figure 2.1 (b). This can also be seen from the energy-band diagram of the structure demonstrated in Figure 2.1 (c). The flow of the majority carriers, electrons here, is blocked by the potential barrier formed by p-Si substrate. When a positive bias is applied from the gate terminal, holes inside the p-Si are repelled from the oxide-substrate interface and a depletion region, where there are no mobile charges, is formed. If the gate bias is increased sufficiently, electrons are attracted to this interface to form a conductive channel region (inversion layer) between the source and drain. This event also can be interpreted as lowering the potential barrier between the source and drain. The

minimum voltage required to reduce the potential barrier and to form a channel layer is defined as threshold voltage, V_T.

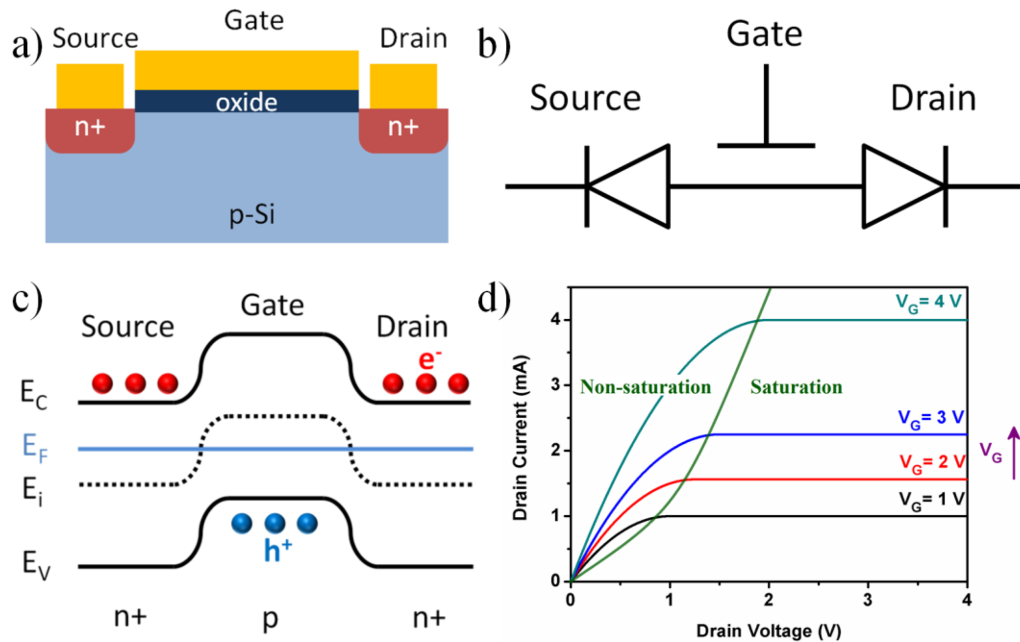

Figure 2.1: A n-channel enhancement mode MOSFET: a) cross section of its structure, b) equivalent circuit in off state , c) Energy-band diagram without bias d) I_D-V_G relation with increasing gate voltage where green line separates saturation and non-saturation regions

For p-channel MOSFETs the channel formation happens for negative gate biases which repels electrons and attracts holes to form a channel. MOSFETs also have two modes of operation depending on the formation of the channel layer at zero gate bias. If there is no channel layer formation (i.e. no drain to source current flow) at zero gate voltage, it is called as enhancement mode device which is normally in the off state. On the contrary, if a transistor has a channel layer (i.e. drain to source current flow) at zero gate voltage, it is called as depletion mode device which is normally in the on state. The enhancement mode devices are more preferred to reduce the power consumption at idle state.

2.1.2 Ideal current-voltage relations for n-channel MOSFET

The derivation of the current voltage characteristics of the MOSFET is beyond the scope of this text, but the relationships will be defined to have a reference for the discussions in the following chapters.

The operation modes of a MOSFET can be separated into three states: off, non-saturation and saturation. When a gate bias lower than the threshold voltage ($V_G < V_T$) is applied, there will be no current flow between source and drain terminals and the transistor operates in the off state (See Figure 2.2 (a)). For a small drain to source bias, V_D, a gate bias larger or equal to the threshold voltage ($V_G \geq V_T$) forms a channel layer as it is shown in Figure 2.2 (b) and the transistor operates in the non-saturation state with a drain to source current (I_D) which is given by,

$$I_D = K_n[2(V_G - V_T)V_D - V_D^2] \qquad (2.1)$$

K_n is the conduction parameter depends and given by

$$K_n = \frac{W}{L}\frac{C_{ox}\mu_n}{2} \qquad (2.2)$$

where μ_n is the mobility of electrons in the channel, C_{ox} is the gate oxide capacitance and W, L are channel width and length, respectively. The ratio of W to L is the main parameter that helps to easily design transistors with different drain currents on the same wafer, whereas other parameters depends on the material properties and changing them requires more effort and cost. As the applied V_D increases, the channel charge density near the drain terminal diminishes. This density becomes zero and the transistor moves to the saturation state when V_D reaches to the saturation drain bias, $V_{D(Sat)}$, which is given by

$$V_{D(Sat)} = V_G - V_T \qquad (2.3)$$

While a transistor is operating in the saturation region, I_D value is given by

$$I_{D(Sat)} = K_n(V_G - V_T)^2 \quad (2.4)$$

As V_D becomes larger than $V_{D(Sat)}$, the point where the channel carrier density is zero, shifts towards to the source terminal. Between this point and the source, there is a voltage drop of $V_{D(Sat)}$. The region between this point and the drain terminal is depleted from mobile carriers and the electrons injected from the edge of channel layer are collected by the drain with the help of the electric field towards the drain. This mechanism and the shape of the channel layer are also shown schematically in Figure 2.2 (d).

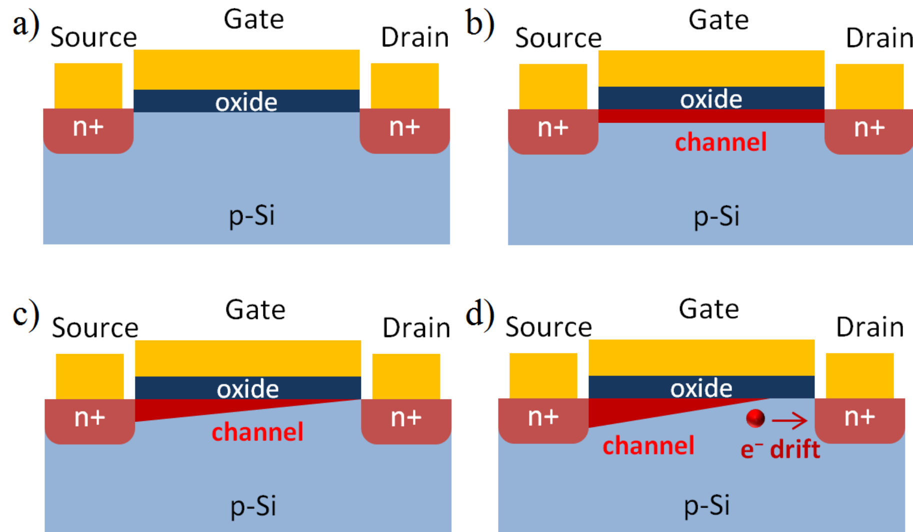

Figure 2.2: Cross sections of n-channel enhancement mode MOSFET for the operation modes of a) off, b) non-saturation, c) transition between nonsaturation and saturation, d) saturation.

2.1.3 Thin Film Transistors

A thin-film-transistor (TFT) is a special kind of MOSFET which has thin channel, oxide and contact layers deposited over a non-conductive and supporting substrate. Unlike MOSFETs where the channel layer is formed inside the substrate (Si), TFTs have a semiconductor film deposited as a channel layer and the substrate is used for physical support. Typically, cheap and transparent

glass substrates are preferred in TFTs. Moreover, plastic substrates (e.g. PET) are used to design flexible TFTs.

TFTs have four different architectures depending on positions (i.e. top and bottom) of gate and contact layers. In this study, the bottom-gate-top-contact architecture, demonstrated in Figure 2.3, is used. For an n-channel enhancement mode TFT structure, an n-type semiconductor with low conductivity is used as the channel layer. The contact metals have ohmic contacts directly to the channel material without highly doped n regions.

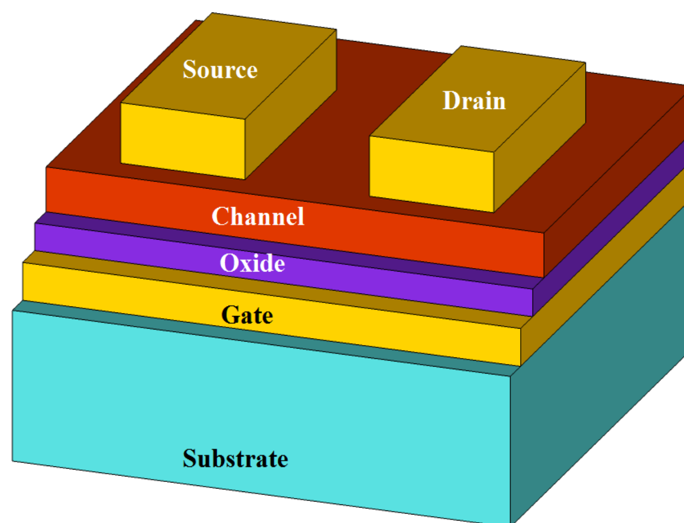

Figure 2.3: A bottom-gate-top-contact TFT architecture, used in this study.

The same current-voltage relations defined for MOSFETs are also valid for TFTs. For an n-type enhancement mode TFT, a positive gate bias attracts electrons from drain and source terminals to the channel layer and increase the conductivity of channel. Whereas, a negative gate bias repels electrons from the channel and decreases its conductivity.

2.2 Semiconductor Photodetectors

A semiconductor photodetector is an optoelectronic device that converts the incident optical signal to an electrical signal. The operation principle of a semiconductor photodetector (i.e. photodetection mechanism) can be divided into two main steps: (i) absorption of photons by a semiconductor and electron hole pair generation, (ii) drift of these charge carriers with an electric field and collection of these charges at contacts (See Figure 2.4).

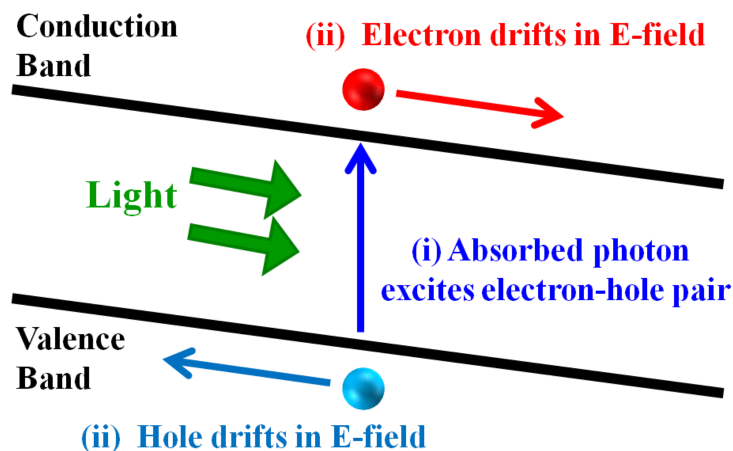

Figure 2.4: Photodetection process in the semiconductor photodetectors: (i) absorption of incident photon, (ii) separation and drift of electron-hole pair and collection of drifted charge carriers.

For the absorption of an incident photon, it should have sufficient energy to excite an electron from one state to another inside the semiconductor. Typically, this excitation occurs from valence band to conduction band of semiconductor and it is called intrinsic or band-to-band absorption as shown in Figure 2.5 (i). The intrinsic transition requires a photon with a minimum energy equals to the band gap of the semiconductor. In semiconductors with crystallographic defects, which act as donor or acceptor defect states in the forbidden band gap, there is also a sub-band gap absorption mechanism. This mechanism is coined as extrinsic absorption mechanism which is the excitation of an electron (ii) from

the valence band to a defect state or (iii) from a defect state to the valence band (See Figure 2.5).

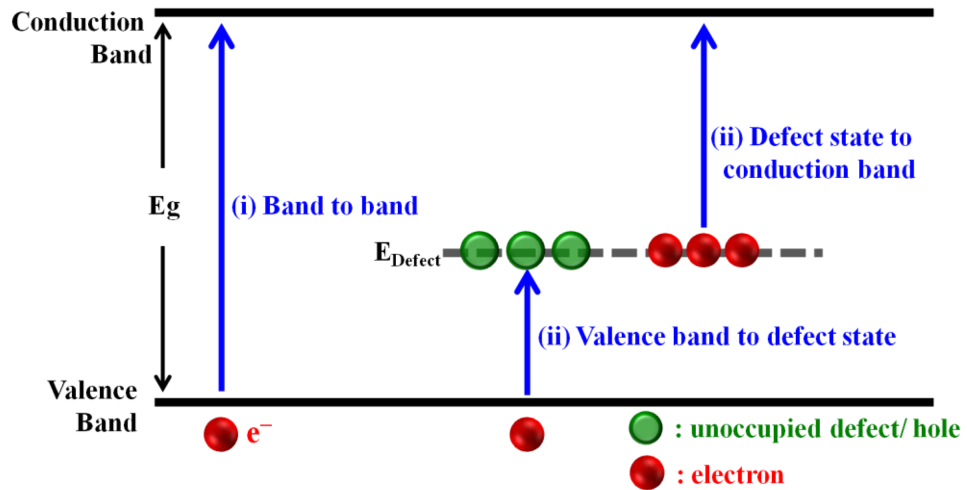

Figure 2.5: Photoexcitation mechanisms: (i) from valence band to conduction band, (ii) from valence band to defect state, and (iii) from defect state to conduction band.

After the generation of charge-carrier (i.e. electron-hole) pair, the electric field in the semiconductor pushes electron and hole away from each other. The photodiodes have an either p-n, p-i-n or Schottky junction to generate a built-in electric field which would separate charges. On the other hand, in photoconductors, an external bias is applied to create an electric field in the semiconductor and separate the charges. When the photogenerated electrons and holes are separated in the semiconductor, the electric field drifts them towards anode and cathode contacts which complete the photodetection process.

2.2.1 Photoconductors

The semiconductor photodetectors can be separated as photodiodes and photoconductors in terms of having a junction and built-in potential. The photodiodes have a junction (i.e. p-n, p-i-n or Schottky) to separate and collect the photogenerated charges. They are commonly used in industrial applications due to their high performance and low cost. On the contrary, the

photoconductors do not have such a junction and they are based on photoconductivity, which is the variation of conductivity of a semiconductor when it is exposed to light. When it is compared with photodiodes, it is easy to fabricate a photoconductor which is simply a slab of semiconductor with two ohmic contacts. The semiconductor in photoconductors is usually deposited with relatively simple processes like thermal evaporation and sputtering.

2.2.2 Photoconduction and photoconductive gain

When an incident photon is absorbed in a semiconductor layer, it generates a charge-carrier (electron-hole) pair and they are separated and drifted towards contact regions with the applied electric field. The applied electric field is calculate as,

$$E = \frac{V}{L} \tag{2.5}$$

where V is the applied voltage bias and L is the distance between the ohmic contacts. The drift speed of charges are given by,

$$v_{n,p} = \mu_{n,p} E \tag{2.6}$$

where $\mu_{n,p}$ is the mobility of electron and hole. The charges are collected by the contacts in the drift time which is given by,

$$T = \frac{L}{v_{n,p}} \tag{2.7}$$

In defect-free semiconductors, for each absorbed photon, a pair of charge carriers contributes to the current flow and the quantum efficiency, η, is near unity. However, photoconductors are fabricated using simple and fast techniques which results in either polycrystalline or amorphous semiconductor layers that have recombination and trap centers. The grain boundaries and interfaces are the main source of recombination centers, whereas crystallographic defects and surface states cause trap centers. The recombination centers reduce the quantum efficiency since the generated charge pair recombines before reaching to a

contact and more than one electron-hole pair is required to complete a single drift cycle. On the other hand, the trap centers lead to a photoconductive gain which significantly improves the quantum efficiency.

In addition to the intrinsic (band-to-band) absorption mechanism, the trap centers introduce an extrinsic absorption mechanism which is the excitation of an electron form valence band to a trap state (electron trapping) or from trap state to conduction band (hole trapping).

Consider an electron is excited from valence band to a trap center; it will be captured in this center for a characteristic release time of τ_n. The hole left behind is collected with the applied bias. The trapped electron results in a net charge in the material. Then, to keep charge neutrality, a hole will be injected from the anode into the semiconductor. The injected hole also drifts towards the cathode under the influence of the applied electric field. The drifting hole has a very slim probability to encounter with the trapped electron which is spatially localized to the defect. Once the hole is collected at the cathode, the same charge injection and drift cycle will repeat, until the trapped electron is released and reach to the anode. Therefore, the trapped electron completes one cycle whereas injected holes complete m cycles where m is given by,

$$m = \frac{\tau_{n,p}}{T} \tag{2.8}$$

As a result, a photoconductive gain is achieved in photodetector and it is given by,

$$M = 1 + m = 1 + \frac{\tau_{n,p}}{T} = 1 + \frac{\tau_{n,p}\mu_{n,p}V}{L^2} \tag{2.9}$$

The photoconductive gain expression depends on applied bias (V) and the square of the distance between ohmic contacts (L^2). In the following chapters, L is going to correspond to the channel length of our TFTs and V is going to be

the drain to source voltage bias. To sum up, the conductance of the semiconductor slab, G, is given by,

$$G = \frac{I_{dark} + MI_{ph}}{V} = G_{dark} + \frac{\left(1 + \frac{\tau_{n,p}\mu_{n,p}V}{L^2}\right)I_{ph}}{V} \qquad (2.10)$$

Where I_{dark} is the dark current and I_{ph} is the photocurrent term corresponding to single cycle of charge carriers (i.e. photocurrent without considering photoconductive gain). For M >> 1,

$$G = G_{dark} + \frac{\tau_{n,p}\mu_{n,p}}{L^2}I_{ph} \qquad (2.11)$$

For a mechanically chopped illumination, the dark conductivity term, G_{dark}, becomes the static component of the conductivity and the second term becomes the alternating component of the conductivity which can be measured with lock-in technique. Therefore, in the following chapters, the alternating part of the conductivity or the current, which is the multiplication of conductivity and the drain to source bias, is going to be measured. It is also important to note that this term has $1/L^2$ dependency.

2.2.3 Photo-Thin-Film-Transistor

As it is mentioned before, a photoconductor is a slab of semiconductor with two ohmic contacts, whereas the drain/channel/source structure of TFTs has the same formation. Therefore, a TFT with a light absorbing channel layer has a photoconductor structure with an additional gate terminal. A photo-TFT is a three-terminal optoelectronic device which can be described as a gated-photoconductor or a TFT with photoresponse. The third terminal (i.e. gate) provides an additional control over the photoresponse of TFTs by controlling the number of mobile electrons or holes inside the light absorbing channel layer. Jeon et. al. previously reported such an additional gate terminal to improve the speed of IZO based photoconductors [41]. In this thesis, the third terminal is

used to tune the photoresponse of ZnO channel by controlling the occupancy of the defect states.

2.3 Defect characteristics of ZnO

When ZnO is optically excited with UV photons which have energy greater than its band gap (3.37 eV), ZnO emits light in a broad wavelength spectrum. In the literature, the investigation of its emission mechanisms is conducted in three wavelength regions: violet-blue, green and orange-red. These sub-band gap emission mechanisms are generally linked to crystallographic defect states of ZnO. Nevertheless, there are also reports that claim impurity atoms are also responsible for these emissions [42]. In our study, ZnO layers are not intentionally doped with impurity atoms and also XRD and XPS characterizations of the same ZnO layers (reported by Oruc et. al.) do not show any extra peaks other than the expected ZnO peaks [43]. Therefore, only intrinsic defects are discussed in this thesis. For a detailed review of the emission mechanisms from impurity atoms, the book of Morkoc et. al. is a useful resource [44].

2.3.1 Violet - blue emission:

The least controversial emission mechanism of ZnO is the ultraviolet light emission mechanism which is the radiative recombination of its excitons [39]. The transition is also shown schematically in Figure 2.6 (i). Since it is not defect related, it can also be observed in stoichiometric samples with very high crystal quality [45, 46]. Moreover, this emission peak is also helpful to determine the crystal quality of ZnO layer [47]. As the crystal quality of ZnO layer decreases, the emission intensity weakens and observing this emission becomes more difficult.

The energy level of Zinc interstitial defects, Zn_i, is reported as 0.22 eV below the conduction band [1, 40, 45, 46, 48]. The transition from this state to the valence band emits violet light around 3.15 eV (See Figure 2.6 (ii)). However, Ahn et. al. reported that this transition disappears at temperatures above 100 K since Zn_i to oxygen vacancy, V_O, becomes the dominant transition with the increasing temperature [40]. Thus this emission can only be observed in low temperature photoluminescence measurements.

Normally, the majority of defect centers of ZnO are Zn_i and V_O which also make it n-type material. However, by controlling deposition parameters especially increasing the oxygen concentration during deposition, it is possible to have Zinc vacancies (V_{Zn}) and Oxygen intersitials (O_i) [40]. It is reported that V_{Zn} states are placed 0.3 eV above valence band [49, 50]. The transitions from conduction band to V_{Zn} and from Zn_i to V_{Zn} emit light at 3.07 eV (violet) and 2.85 eV (blue), respectively. These transitions are also shown schematically in Figure 2.6 (iii) and (iv).

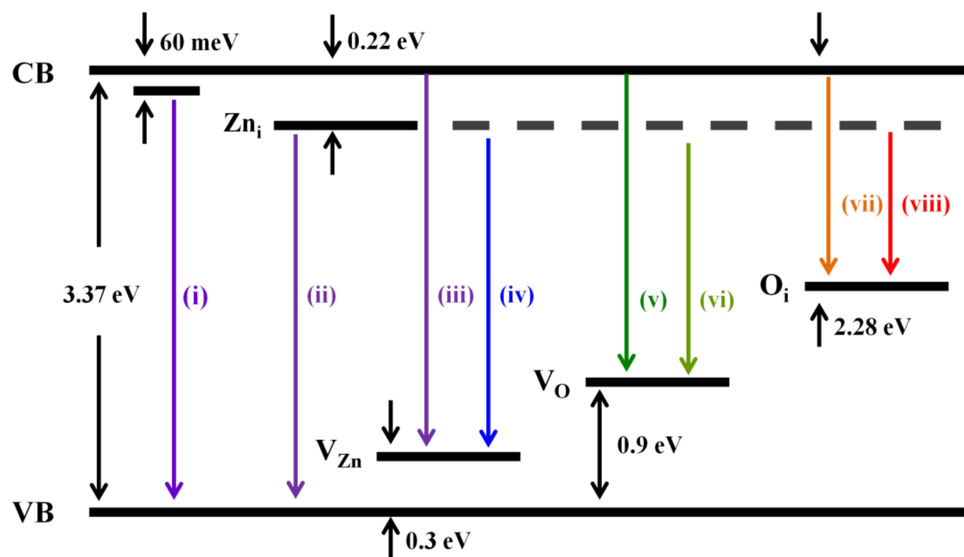

Figure 2.6: Energy band diagram that shows the energy levels of crystallographic defects of ZnO reported in the literature.

2.3.2 Green emission:

It is calculated that oxygen vacancies (V_O) are located 0.9 eV above the valence band [51]. It is experimentally shown that the green emission is due to the transitions from conduction band to V_O and from Zn_i to V_O which emits green light at 2.47 eV and 2.25 eV. These transitions are shown in Figure 2.6 (v) and (vi).

In their analysis on ZnO layer deposited with magnetron sputtering, Ahn et. al. showed that increasing number of Zn_i and V_O defect state increases both carrier concentration, and green emission of ZnO [40]. Vempati et. al. also reported that as the temperature increases (especially for $T > 150K$) the transition from Zn_i to V_O blueshifts toward the transition from conduction band to V_O since electrons start to localize in higher states [39].

2.3.3 Orange-red emission:

Intersitial oxygen (O_i) states are the main source of the orange-red emission characteristics in ZnO. They are located 2.28 eV below the conduction band [49, 52, 53]. The transitions from CB to O_i and from Zn_i to O_i emit light at 2.28 eV and 2.06 eV as shown in Figure 2.6 (vii) and (viii).

Chapter 3

Experimental Methods

This chapter describes the fabrication of ZnO based photo-TFTs and the major characterization methods in this study. The experiments are conducted in UNAM Cleanroom Facilities (UCF) (class 100 and 1000) and Okyay Group Laboratories in UNAM at Bilkent University. The device fabrication consists of four main steps: i) surface preparation, formation of ii) isolation layer, iii) gate stack, and iv) electrical contacts. Characterization methods involve photoluminescence measurements and spectral responsivity measurements.

3.1 Device Fabrication

3.1.1 Surface preparation

ZnO TFTs are fabricated on highly doped (10-18 mΩ·cm) p-type (111) Si wafer, in a back gate configuration. The following wafer cleaning procedure, similar to the RCA (Radio Corporation of America) cleaning procedure is conducted to

remove organic and inorganic contamination at the Si wafer surface. Clean and hydrophobic (H-terminated) Si wafer surface is achieved.

In order to remove organic contaminations, the wafers are cleaned in H_2SO_4:H_2O_2 (4:1), piranha solution, for 10 minutes. Then, the samples are rinsed in DI water and dried with N_2 gun.

While the piranha solution etches organic contaminations, it oxidizes the Si surface. To remove this thin oxide layer and other inorganic contaminations, the samples are cleaned in buffered oxide etchant (BOE 7:1, NH_4F:HF) until the Si surface became hydrophobic under visual observation. Then, the samples are rinsed in DI water and dried with N_2 gun.

3.1.2 Formation of the isolation layer

In order to prevent the leakage from source and drain contacts to gate (Si substrate) a thick isolation layer is required between Si wafer and source-drain contacts. For this purpose, 200-nm-thick SiO_2 layer is deposited using VAKSIS CVD-Handy Plasma Enhanced Chemical Vapor Deposition (PECVD) system. The deposition is conducted at 250 °C with a chamber pressure of 1 torr and RF power of 10 W. N_2O and SiH_4 are used as precursors with flow rates of 15 sccm and 6 sccm, respectively. As carrier gas, He is used with 700 sccm flow rate.

The active device area is patterned by photolithography and wet oxide etching. Initially, to improve adhesion of the photoresist, HMDS (hexamethyldisilazane) is spin coated at 4000 rpm for 40 seconds. AZ5214E is spin coated at 4000 rpm for 40 seconds; which resulted in 1.4-µm-thick photoresist layer. The samples are prebaked at 110 ºC for 60 seconds and exposed to UV light. Then, UV exposed regions are developed using AZ400K:H_2O (1:4) solution for 30 seconds. In order to improve the chemical stability of the photoresist layer, the samples are hardbaked at 120 ºC for 2 minutes.

After defining active regions, the SiO_2 layer in these regions is etched using BOE for 10 minutes (See Figure 3.1). Sample is rinsed with DI water and remaining photoresist is removed by sonicating in acetone.

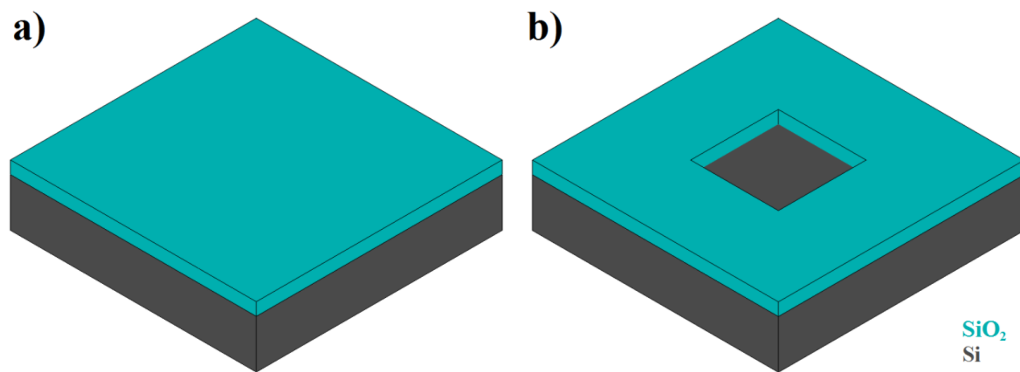

Figure 3.1: In order to reduce leakage between gate and top contacts, 200-nm- thick SiO_2 layer is deposited (a) and patterned (b) to define active regions

3.1.3 Formation of the gate stack

The gate oxide and channel layers are deposited using ALD technique (Cambridge Nanotech Savannah 100 ALD System). The interface between back gate Si substrate and gate oxide is important to prevent possible charging and leakage problems. Therefore, the samples are immediately loaded into the ALD chamber. As gate oxide, 200 cycles of (20-nm-thick) Al_2O_3 layer is deposited at 250ºC using trimethylaluminum and water vapor precursors (See Figure 3.2 (a)).

As the channel layer, ZnO film is deposited for 100 ALD cycles (14-nm-thick) as shown in Figure 3.2 (b). Diethylzinc (DEZ) and water precursors are used to deposit ZnO. The deposition temperature is varied from 80°C to 250ºC in our fabrications to analyze its effect on optical performance of ZnO TFTs. The pulse and purge times of ZnO film deposition are given in Table 3.1. The standard recipes provided by Cambridge Nanotech are used for 80, 200 and 250 °C. As the deposition temperature increases, precursors become more energetic and the

required time for depositing single layer decreases. In order to stay in the safe side, the recipe designed for 80 °C is also used at 100 and 120 °C. The material characteristics of the ZnO layer are previously reported by Oruc et. al. [43].

Table 3.1: ALD recipes for depositing ZnO at various temperatures

Growth Temperature	DEZ pulse	Purge Time	Water pulse	Purge Time
80 °C	0.015 s	60 s	0.015 s	60 s
100 °C	0.015 s	60 s	0.015 s	60 s
120 °C	0.015 s	60 s	0.015 s	60 s
200 °C	0.015 s	10 s	0.015 s	10 s
250 °C	0.015 s	5 s	0.015 s	5 s

The channel region is patterned by previously described photolithography technique (without the final hardbake step) and wet etching. ZnO layer is etched using diluted H_2SO_4:H_2O (2:98) solution. The ALD deposited Al_2O_3 layer is not etched on purpose, which improves isolation by filling pinholes in thick PECVD-deposited SiO_2 layer (See Figure 3.2 (c)). The remaining photoresist is removed by sonicating samples in acetone. The samples are rinsed with isopropanol, DI water and dried with N_2 gun.

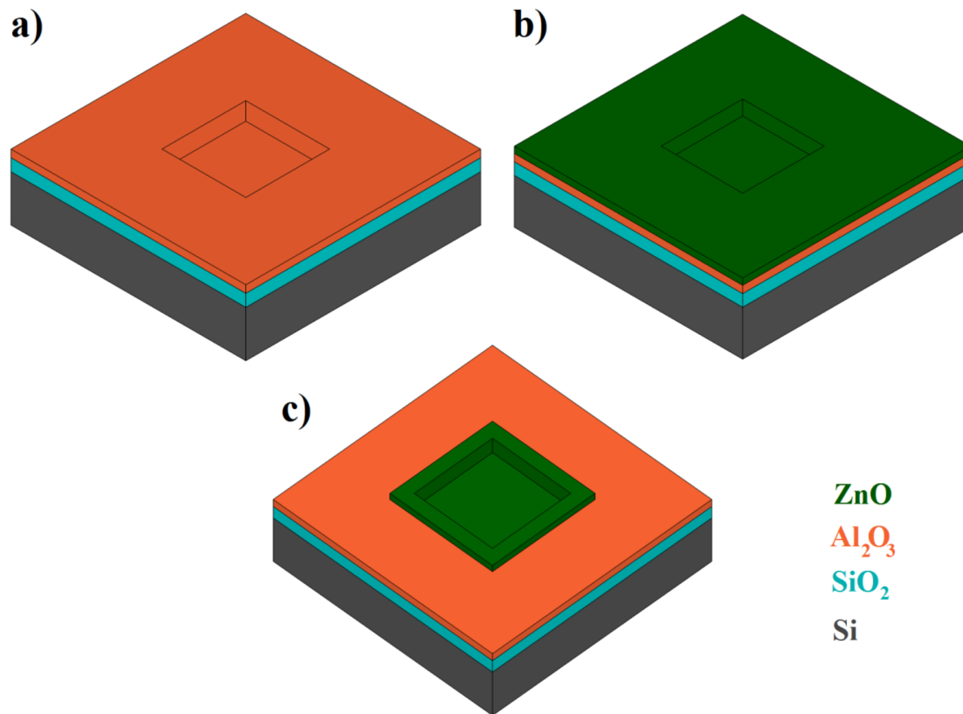

Figure 3.2: Deposition of gate oxide and channel layers. a) 20 nm thick Al_2O_3 and b) 14 nm thick ZnO deposited using ALD technique. c) The deposited ZnO layer is patterned with lithography and diluted H_2SO_4 wet etch solution.

3.1.4 Formation of the electrical contacts

As source and drain contacts, Al contact pads are formed using the following lift-off procedure. Initially, the contact regions are defined by photolithography. Then, 100-nm-thick Al is evaporated using VAKSIS PVD Vapor 3S Thermal Evaporator with 0.6 Å/sec deposition rate at 10^{-6} Torr. Finally, the samples are sonicated in acetone to complete the lift-off process (See Figure 3.3 for the schematic of completed device). The samples are rinsed in isopropanol, DI water and dried with N_2 gun.

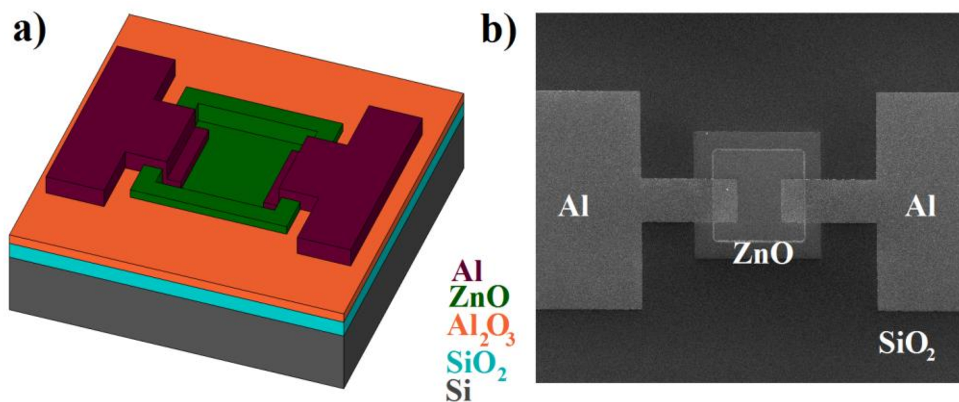

Figure 3.3: 100 nm thick Al layer deposited and patterned using lift-off technique to form source and drain contacts. a) Schematic of a finalized TFT design. b) A microscope image taken from a sample after the lithography step which defines source and drain contact regions.

3.2 Characterization methods

3.2.1 Photoluminescence measurements

Photoluminesence (PL) is light emission initiated by an optical excitation. In this study, PL data is used to understand the energy levels of defect states inside the ZnO channel layer. PL data is taken using Cary Eclipse Fluorescence Spectrophotometer. The schematic of typical PL measurement setup is shown in Figure 3.4. The output of a wide band light source (Xenon lamp) is monochromated by the excitation monochromator and then it passes through the excitation slit. The sample cell is placed in the path of the monochrome light with an angle close to 45°. While placing the sample, it is important not to send the reflected excitation light directly to the emission slit. Such an alignment can be easily done by setting excitation wavelength to 550 nm and checking that reflected light is not directed to the input of the emission slit. When the sample is optically excited, it emits light in all directions at various wavelengths depending on its band gap and defect states. A small portion of the emitted light passes through the emission slit and then it is filtered by the emission monochromator. Typically, the remaining optical signal has a very low

intensity; hence a PMT (photomultiplier tube) detector is used to measure such low intensities. To get the spectral distribution of the emitted light, the emission monochromator scans the desired wavelength spectrum and the light intensity measured by the detector is recorded.

In order to obtain PL data from the ZnO layer, ZnO is deposited on double side polished quartz substrates. Our TFT samples are not used because their ZnO coated surface area is much smaller than the beam size of the excitation light and also additional PL signal that may come from the Si substrate or the Al_2O_3 layer may complicate the analysis. A quartz substrate is chosen since it is transparent around excitation wavelengths (250-400 nm) and it does not have PL signal at these excitation wavelengths. To reduce contamination related PL data in our measurements, quartz substrates are cleaned with a piranha solution as previously described. The final step of cleaning procedure, BOE cleaning, is skipped since it would etch quartz substrate. After the surface preparation, 300 ALD cycles of ZnO is coated at various temperatures.

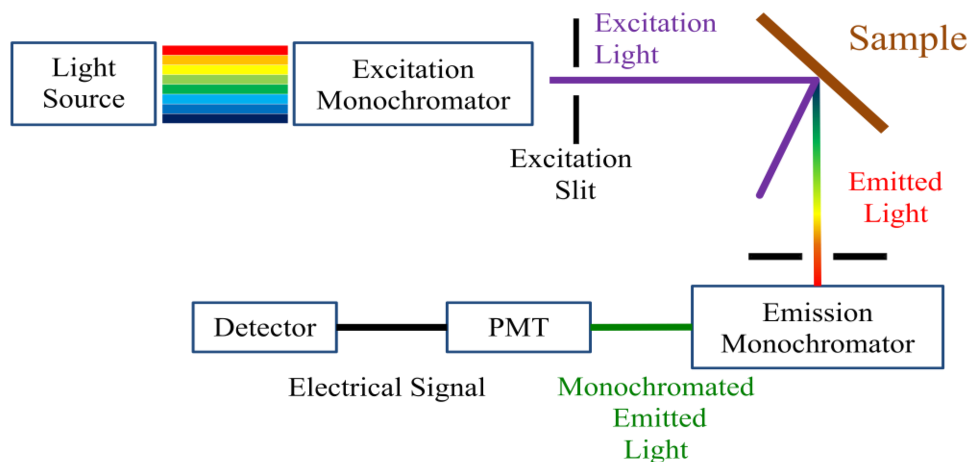

Figure 3.4: Schematic of a typical photoluminescence measurement setup

3.2.2 Spectral photoresponsivity measurements

The photoresponsivity of an optoelectronic device is the electrical output per the optical input. It is calculated as the ratio of the photocurrent to the incident optical power. Spectral responsivity measurements of the fabricated TFTs are conducted with the experimental setup shown in Figure 3.5. A 150 W Xenon lamp is used as a wideband illuminating source. Monochrome light (Oriel 1/8 m Cornerstone Monochromator, 1200 lines/mm grating) is obtained and mechanically chopped at 395 Hz. The light is focused on the fabricated device from the top at normal incidence. The source and drain terminals of TFTs are biased with a Keithley 2400 sourcemeter. The gate terminal voltage bias is independently controlled with a separate voltage supply (Keithley 2400).

A lock-in amplifier (Stanford Research Systems 830) is used to measure the photogenerated current between the source and drain terminals. Ideally, connecting a lock-in amplifier in series and measuring the photocurrent is prefered. However, in the series mode, the current measurement mode, our lock-in amplifier has a maximum allowed current limit, 10 μA, which is much less than the current passing between source and drain terminals in the accumulation mode of our transistor. Therefore, a 1 kΩ resistor is connected in series between the drain terminal of our transistor and the ground port of the voltage supply and the voltage drop on this resistor is measured by the lock-in amplifier. In the worst case, the accumulation mode, the resistance between source and drain terminals is about tens of kΩ which is at least ten times greater than the connected 1 kΩ resistor. Therefore, most of the applied drain to source voltage bias, V_{DS}, still appears across our TFTs instead of the connected resistor and the applied drain to source voltage bias is reported in this study. Incident optical power at each measurement wavelength is recorded by a calibrated Si photodetector.

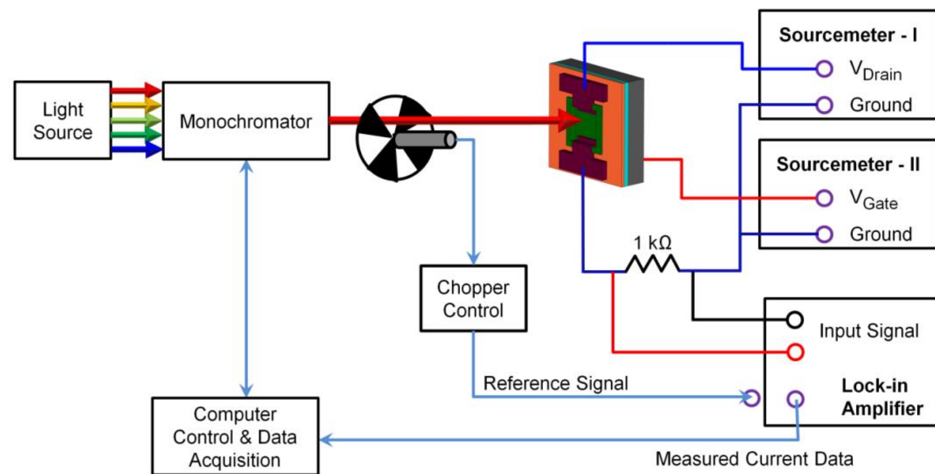

Figure 3.5: Responsivity measurement setup. Monochrome light is focused on the fabricated device from the top at normal incidence. The photocurrent between drain and source terminals is measured with a lock-in amplifier.

A Lab-View code is used to automate the spectral responsivity measurements. Initially, the code sets lock-in amplifier (time constant: 1 sec, sensitivity: 50 μV), sourcemeters (gate and source biases) and monochromator (initial wavelength: 250 nm) to desired measurement parameters and it waits for 5 time constants to stabilize the system. After the stabilization, to minimize transient experimental errors, 8 consecutive photocurrent measurements with 0.5 sec time delay between each other are taken. Then, the monochromator is set to the next desired wavelength and again measurements are taken after the stabilization. When desired wavelength spectrum is completely scanned, the next desired gate and source biases are set and the same measurement procedure is followed. The spectral responsivity is computed as the average of 8 measurements at each wavelength divided by the previously recorded normalized incident optical power at that wavelength.

The incident optical beam spot (on the surface of the sample) is 400 μm wide and 1200 μm long. The calibrated Si photodetector (Newport 918D-UV-OD3R) has 1.13 cm long active detection diameter which is much larger than the beam spot and it can measure the total incident power. On the other hand, the channel

region sizes of our devices are smaller than the beam spot. In order to calculate responsivity values accurately, the measured optical power is normalized to the device size.

Our monochromator uses a diffraction grating to generate a desired monochromatic light from the incident white light. However, when the light is reflected from a diffraction grating, a polychromatic light is generated. In addition to the desired wavelength (λ), this polychromatic light also includes second (λ/2), third (λ/3) and larger harmonics (λ/n) of the target wavelength [54-56]. In order to eliminate these higher order harmonics, a long pass filter at 500 nm (Newport FEL0500) is used in our measurements for the wavelengths longer than 550 nm. The spectral distribution of the total incident optical power with and without the filter is shown in Figure 3.6. To reduce the measurement time and complexity, most of our measurements are done for the wavelength range from 320 nm to 600 nm where the higher order harmonics do not affect our measurements. A closer view of the incident optical power in this spectrum is plotted in Figure 3.7.

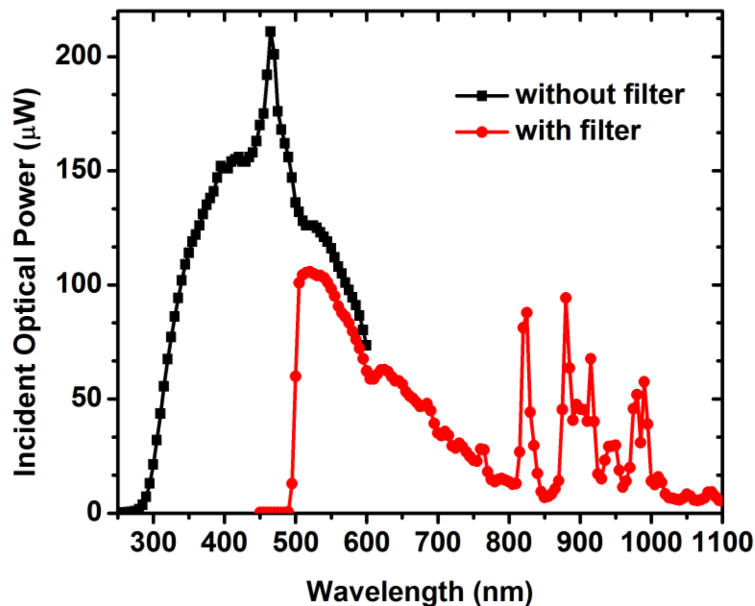

Figure 3.6: Incident optical power measured by calibrated Si photodetector with and without a long pass filter at 500 nm.

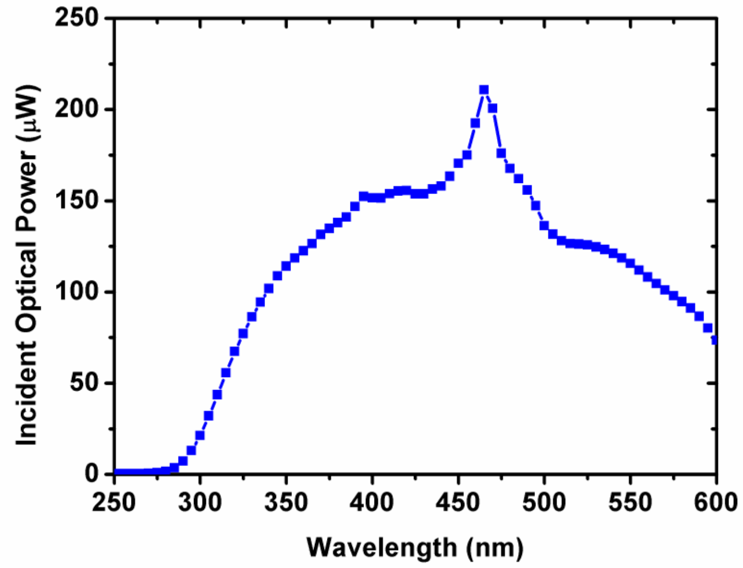

Figure 3.7: Incident optical power measured by calibrated Si photodetector without a long pass filter at 500 nm.

Chapter 4

Results and discussions

This chapter presents the experimental study of ZnO based photo-TFTs with an actively tunable photoresponse in the visible region. The chapter begins with analyzing basic operation principles of fabricated TFTs. Then, the energy levels of crystallographic defect states in the ZnO channel layer are investigated. After that, the active tuning mechanism and controlling occupancy of trap states are discussed. Finally, the effects of device size and deposition temperature on the photoresponse of ZnO based photo-TFTs are discussed.

4.1 Transistor characteristics

The basic transistor properties such as on/off ratio, threshold voltage and subthreshold slope values of the fabricated ZnO-channel TFTs are investigated. The current-voltage (I-V) measurements are taken using a parameter analyzer (Keithley 4200 SCS) and a manual probe station (Cascade Microtech PM-5) in a dark environment.

ZnO TFTs show n-channel enhancement type transistor characteristics. The drain current of fabricated devices increases with the increasing gate voltage as it is shown in drain current-gate voltage (I_D-V_G) measurements taken from TFTs with a ZnO channel layer deposited at 80 °C (See Figure 4.1). Also, the device exhibits a threshold voltage of 3.79 V and a decent on/off ratio of 10^9.

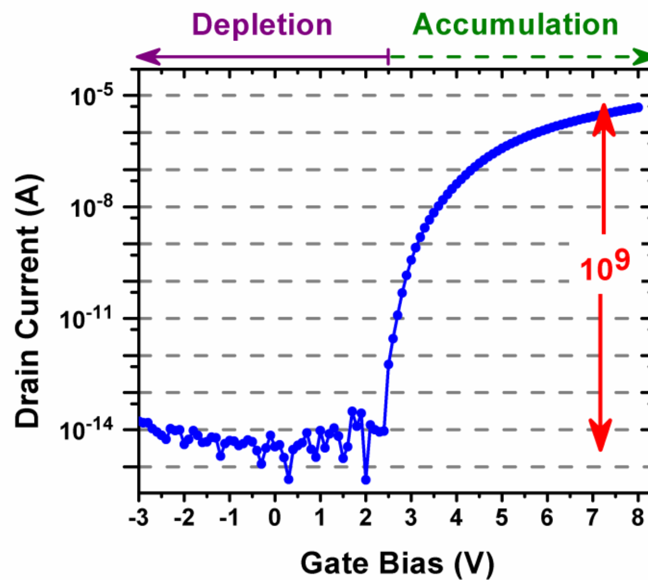

Figure 4.1: I_D-V_G characteristics of ZnO-based TFTs which indicate n-channel enhancement mode transistor characteristics. The device also has a threshold voltage of 3.79 V and a decent on/off ratio of 10^9. The channel layer of measured device is deposited at 80°C and its both channel length and width are 100 µm. 1 V of drain bias is applied.

As it is previously described in the scientific background chapter, the drain current of a transistor linearly scales with the ratio of channel width to channel length. The channel size dependent I_D-V_G characteristics of our devices, shown in Figure 4.2, are in an agreement with the drain current expression given in Equation (2.4). The linear scaling of I_D with channel size is also shown more explicitly in Figure 4.3.

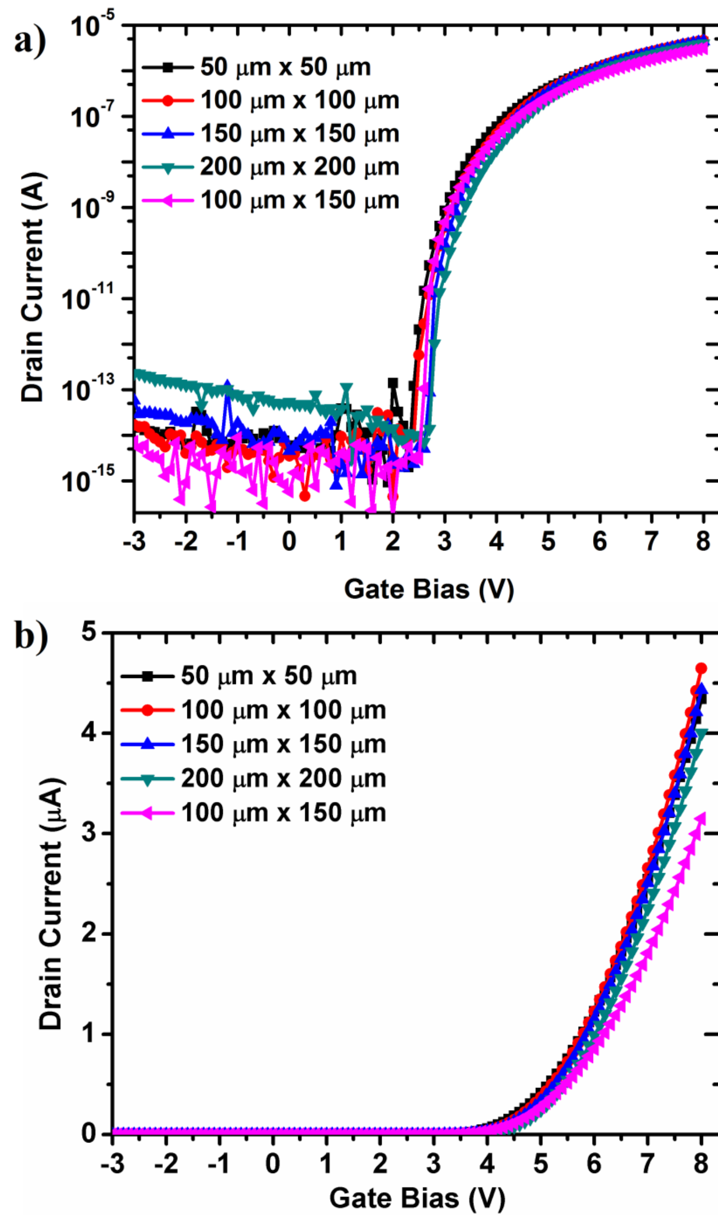

Figure 4.2: I_D-V_G characteristics of devices, having various channel sizes, are shown in (a) logarithmic and (b) linear scale. The sizes shown in the legends are channel width and channel length, respectively. Measurements are taken from devices with a channel layer deposited at 80 °C and 1 V is applied as the drain to source bias.

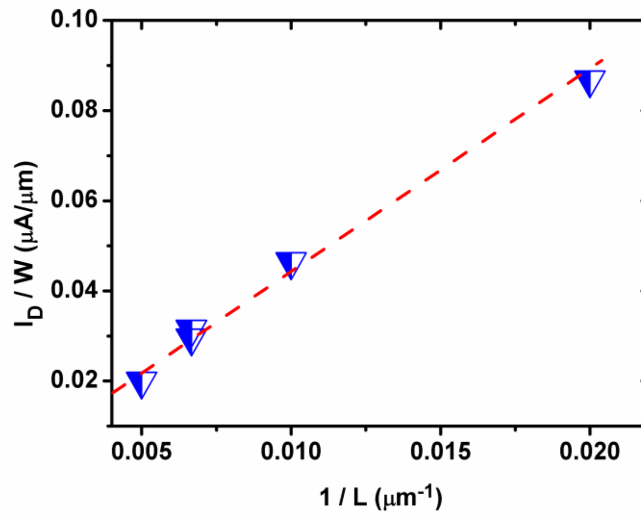

Figure 4.3: Scaling behavior of ZnO based TFTs fabricated at 80 °C. All devices are biased with 1 V drain bias and 8 V gate bias. The dashed red line shows linear drain current scaling characteristics of fabricated TFTs.

To investigate the effects of growth temperature on TFT characteristics, I-V measurements are taken from devices having a ZnO channel layer deposited at different temperatures (See Figure 4.4). In order to keep other parameters constant, devices having same sizes (i.e. 100 μm to 100 μm) are measured under a drain bias of 1 V.

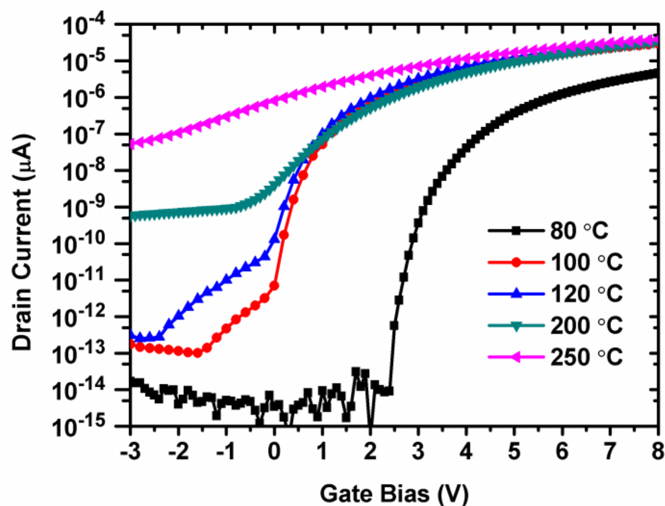

Figure 4.4: I_D-V_G characteristics of devices having ZnO channel deposited at various temperatures

The threshold voltage values of the devices are calculated by using linear extrapolation in the saturation mode [57]. Briefly, $I_D^{0.5}$-V_G curve is plotted and linear region of the plot where the transistors are in saturation mode is linearly extrapolated to zero drain current as shown in Figure 4.5. The gate bias value of the extrapolated line corresponds to threshold voltage at zero drain current.

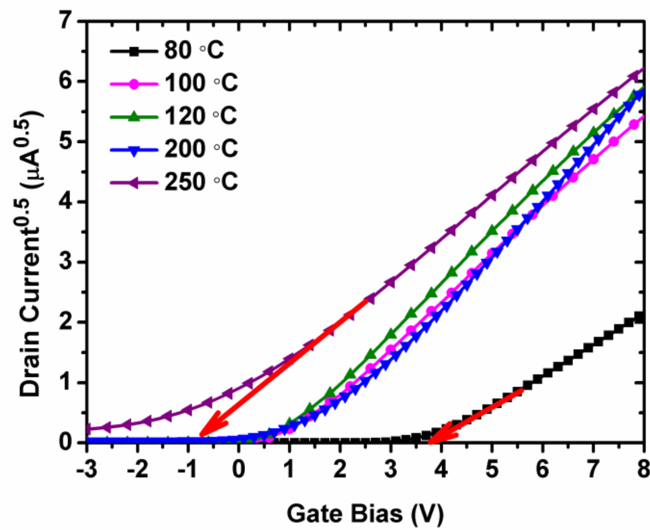

Figure 4.5: Threshold voltage calculation using extrapolation in the saturation region technique. $I_D^{0.5}$-V_G characteristics of devices are plotted and drain current values are linearly extrapolated to zero drain current value.

For ZnO TFTs, on/off ratio values from 10^2 to 10^8 are reported in the literature [13] [58-60]. Among our fabricated devices, the device deposited at 80°C exhibits a very high 10^9 on/off ratio, which is attributed to low ALD growth temperature. Earlier reports show that the transistor on/off ratio increases at lower ALD growth temperatures [59]. This is explained by the reduced electron concentration due to less number of defects in the crystal [61]. The device exhibits decent subthreshold slope of 288 mV/dec. Previously reported subthreshold slope values range from 24.1 to 0.25 V/dec [58-60]. As the deposition temperature increases, the performance of transistors decreases in terms of on/off ratio and subthreshold slope (see Table 4.1). For high temperatures (e.g. 200 and 250 °C), the doping concentration significantly

increases so that it would be hard to deplete such a conductive channel and on/off ratio of transistors decreases for these temperatures. In other words, the devices have less gate control over the conductivity of channel layer due to their high number of defects.

Table 4.1: Fundamental transistor characteristics of ZnO based TFTs

Annealing Temperature (°C)	Threshold Voltage (V)	I_{on}/I_{off} Ratio	Subthreshold Slope (V/dec)
250	-0.72	7.3×10^2	2.634
200	1.55	3.6×10^4	0.948
120	0.88	1.35×10^8	0.669
100	1.06	2.9×10^8	0.519
80	3.79	1.3×10^9	0.288

4.2 Defect state analysis

Photoluminescence (PL) measurement is performed on samples prepared by growing 14-nm thick ZnO at 250 °C on quartz substrates (double side polished) using the same recipe described in Section 3.1.3. Room temperature PL characteristics of ZnO film at λ=290-nm excitation is shown in Figure 4.6. The near band edge PL emission peak is due to the exciton recombinations in ZnO. As it is previously mentioned in Section 2.3, the observation of this peak shows a relatively good crystal formation in polycrystalline ZnO layer. Luminescence in the 450 to 700-nm range corresponds to below-bandgap emission, which reveals the presence of deep level traps within the forbidden band of ZnO. The energy distribution of the trap states in the forbidden band cause a broad emission centered around λ=510 nm (2.43 eV). Two possible trap-assisted routes that would result in the emission of a photon with λ=510 nm (2.43 eV)

are illustrated in Figure 4.7. The first scenario is the capture of a free electron from the conduction band by a trap state (unoccupied trap) (route I), and the second one is the recombination of an electron in a trap state (occupied trap) with a hole in the valence band (route II). The latter predicts trap energy states are located in the forbidden band of ZnO, closer to the conduction band. In such a scenario, incident photons with higher energy than 2.43 eV (but less than the bandgap energy) excite electrons from the valence band directly to trap states. This is followed by light emission (at 510 nm) through route II when excited electrons recombine with holes in the valence band. Figure 4.8 plots PL intensity at a constant emission wavelength (510 nm) for different excitation wavelengths. The figure shows that excitation photons with lower energy than the bandgap of ZnO do not result in luminescence at 510 nm. This evidence supports trap-assisted luminescence through route I, which predicts trap energy states located closer to the valence band. This is in good agreement with earlier observations about the energy levels of point defects, oxygen vacancies, in the forbidden band of ZnO [39, 51].

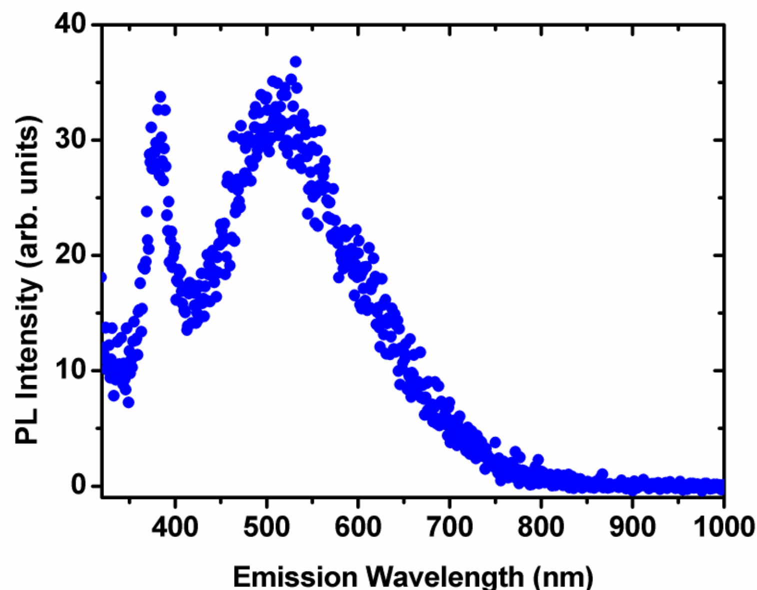

Figure 4.6: Spectral photoluminescence of ZnO layer coated on quartz substrate. Photoluminescence intensity is given in arbitrary units. Photoluminescence excitation wavelength is 290 nm.

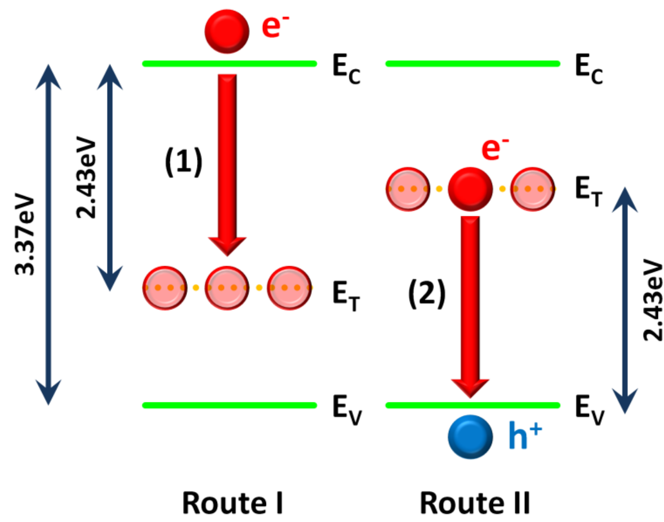

Figure 4.7: Energy level of trap states. Two possible trap-assisted emission routes: Route I: trap energy states are closer to the valence band. Conduction band electrons and localized holes of trap states (unoccupied trap) recombine and emit light (1). Route II: Trap energy states are closer to the conduction band. Localized electrons of trap states (occupied trap) and free holes of valence band recombine and emit light (2).

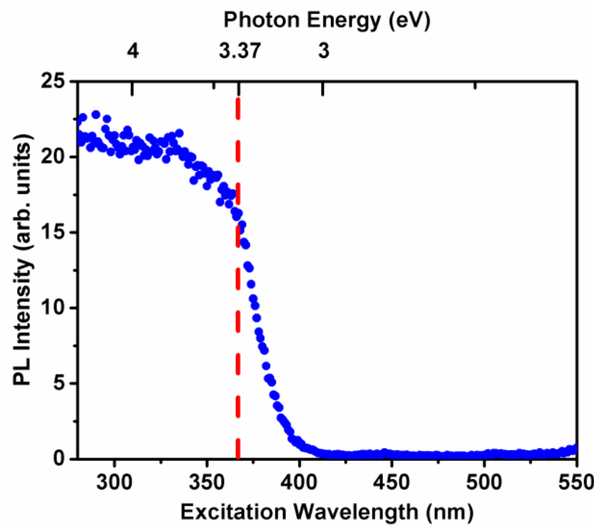

Figure 4.8: Measured photoluminescence intensity at 510 nm (2.43 eV) for various excitation wavelengths. The dashed line shows the bandgap energy of ZnO.

Optical absorption of ZnO film on quartz substrate is also characterized. Measured spectral optical absorption of ZnO (see Figure 4.9) exhibits band-to-band absorption behavior with an excitonic absorption peak located at $\lambda = 365$

nm. Such room temperature excitonic peaks are attributed to large exciton binding energy and are observed in the literature [47]. The dominant photon absorption mechanisms in ALD-grown ZnO are (1) interband and (2) valence band-to-trap state transitions, as depicted in Figure 4.10. Only photons with energies greater than the bandgap of ZnO (i.e., hν = 3.37 eV) are absorbed in an interband transition (1). Whereas photons with energies less than the bandgap can excite valence electrons to empty states at the trap energy level, E_T (2). This process is limited by the availability of unoccupied trap states because the density of states in the valence band is much larger compared to that of the defect states. Photons could also be absorbed exciting electrons from occupied trap states to conduction band (3). However, the rate of this transition is very low since it involves an initially occupied trap state, which is spatially localized.

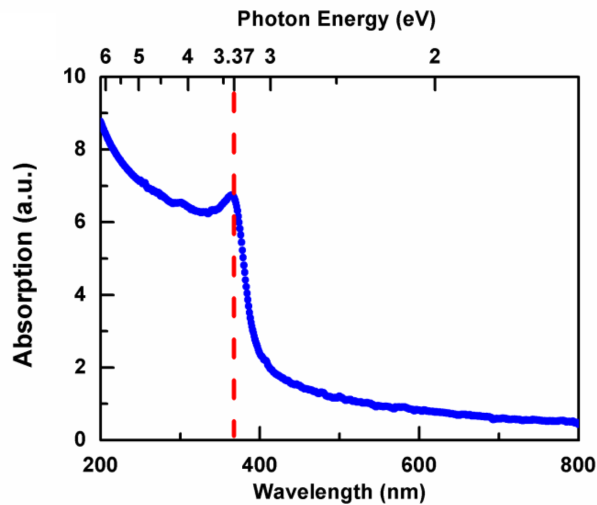

Figure 4.9: Absorption spectrum of ZnO layer on a quartz substrate. Absorption is given in arbitrary units. The dashed line shows the bandgap energy of ZnO.

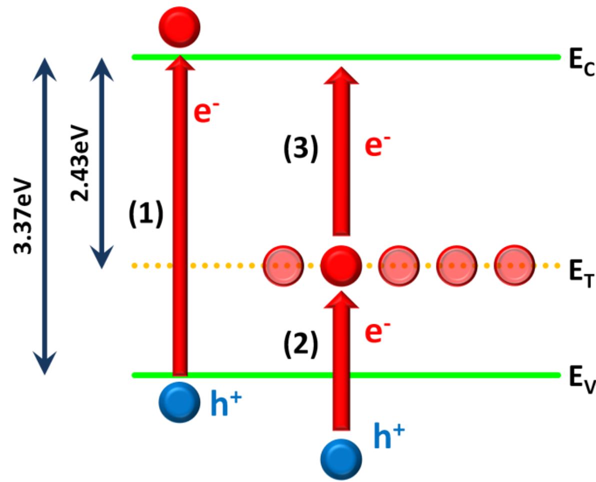

Figure 4.10: Absorption mechanisms of ZnO: Interband (1), valence band to trap state (2), and trap state to conduction band (3).

4.3 Actively tunable photoresponse in the visible spectrum

ZnO band edge is at 3.37 eV; however, lower energy photons can be absorbed through trap-assisted routes, as described in Section 2.2. The magnitude of photocurrent generated by below-bandgap photons depends on the density and availability of proper trap states. Therefore, the photogenerated current in the ZnO channel can be dynamically controlled via changing the occupancy of deep level traps by applied gate voltage bias, as shown in Figure 4.11. The gate voltage bias modifies the depletion region in the ZnO channel and preferentially accumulates or depletes the channel. When the channel is depleted, the deep level states are unoccupied; therefore, strong absorption of subbandgap photons is possible. In the accumulation mode, electrons from the source and drain contacts are attracted to the ZnO channel layer with the applied gate bias, and an accumulated region with a higher electron density, higher conductivity, and higher quasi-Fermi level is formed. As the quasi-Fermi level increases, the trap states are also filled with these extra electrons. Due to the decreasing number of

empty trap states, the subbandgap photon absorption mechanism is prevented. On the other hand, in the depletion mode, applied gate bias repels electrons from the channel region, and the quasi-Fermi level is shifted down. Therefore, the probability of subbandgap photon absorption is boosted by the increase in the number of empty trap states.

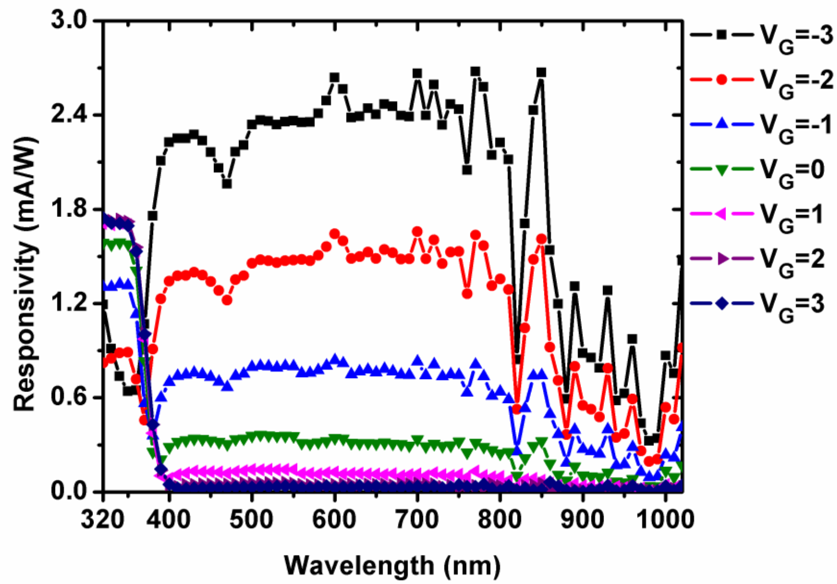

Figure 4.11: Spectral responsivity of a ZnO based TFT at 250 °C with a device size 200 μm x 200 μm and under a drain bias of 3 V.

The excitation of an electron from valence band to trap state requires a photon with a minimum energy of 0.94 eV (~ 1318 nm) as described in Figure 4.10. In our measurements, it is observed that the photoresponsivity of the device begins to decrease for wavelengths longer than 850 nm, which is shown in Figure 4.11.

In our ZnO based photo-TFTs, drain-channel-source (i.e. Al/ZnO/Al) structure can be also evaluated as a photoconductor, which is a slab of semiconductor with two ohmic contacts. Due to its defect states, it has a photoconductive gain mechanism, as it is mentioned in Section 2.2.2. When an electron is excited to a defect state, it will be captured in this trap state for a while. In the mean time, the generated hole is drifted with the applied drain to source bias voltage and collected by the source. To maintain charge neutrality of ZnO layer, another

hole is injected from the drain, but this hole is also drifted and collected by the electric field. Therefore, the photogenerated hole makes multiple passes in ZnO layer, while the electron is trapped. Eventually, the electron is released from the trap center and collected by the drain, which ends this cycle. This photoconductive gain mechanism, significantly improves the performance of ZnO based photo-TFT.

4.4 Effects of the device size on photoresponse to visible light

The effects of device size on responsivity are investigated on ZnO based TFTs fabricated at 250 °C. The measurement results, given in Figure 4.12, show that all of the devices exhibited dynamically controllable photoresponse in the visible spectrum.

The photoconductive gain term has a significant role when the device size is scaled. As it is mentioned in Section 2.2.2, the photoconductive gain is inversely proportional to the square of the channel length, L^2. When the responsivity values are normalized with respect to L^2, shown in Figure 4.13, it is clear that the normalized measurement results have a similar trend. However, higher normalized responsivity values are achieved in devices with shorter channel lengths. One possible reason of such a performance improvement is that the photogenerated carriers are collected more efficiently before they recombine in short channel devices. On the other hand, the photogenerated charges must travel longer distances to contribute to the photocurrent at long channel devices, so their recombination probability before reaching to a metal contact increases.

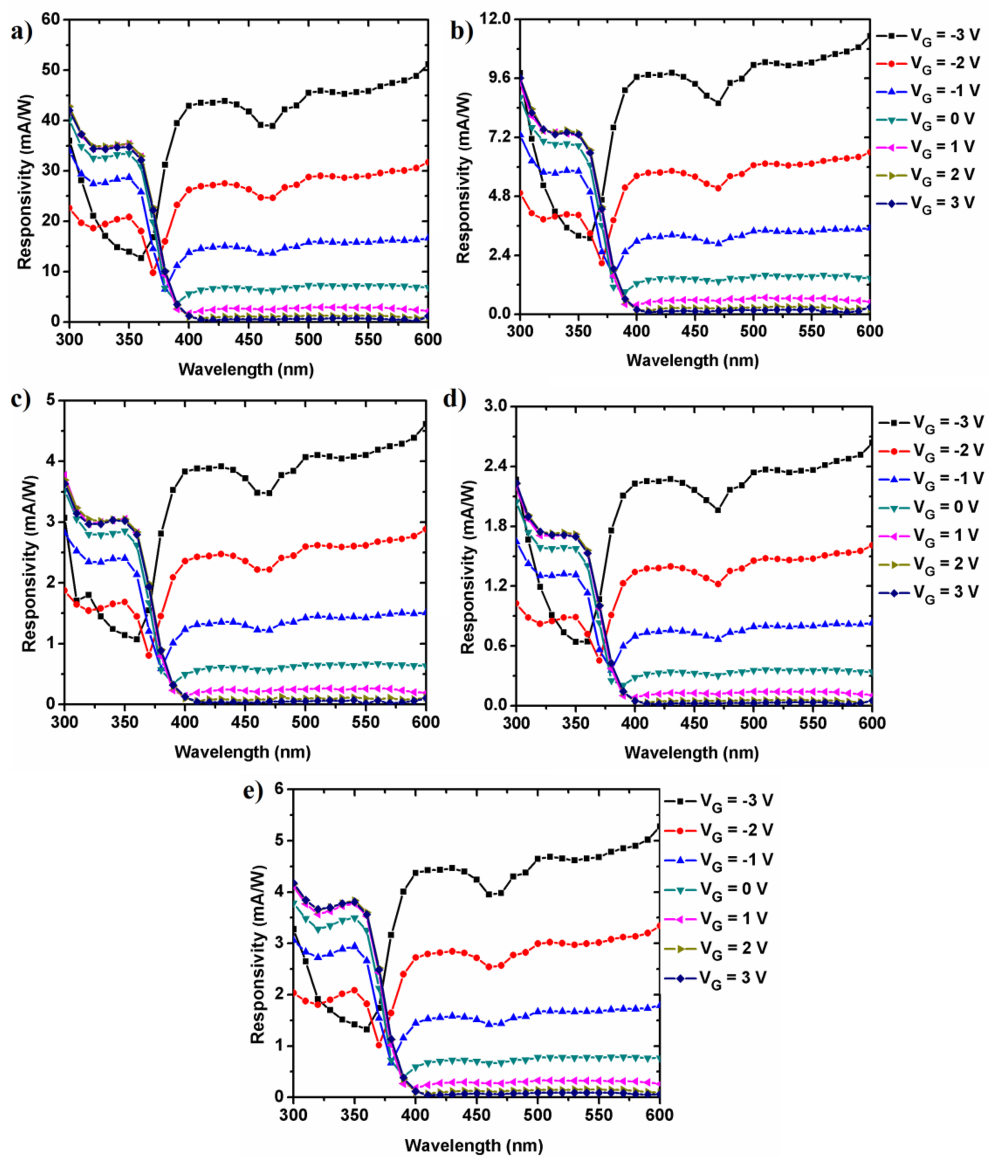

Figure 4.12: Spectral responsivity of a ZnO based TFT at 250 °C for various device sizes while constant V_D bias of 3 V is applied. Corresponding device channel lengths and widths are a) 50 µm - 50 µm, b) 100 µm - 100 µm, c) 150 µm - 150 µm, d) 200 µm - 200 µm, e) 150 µm - 100 µm.

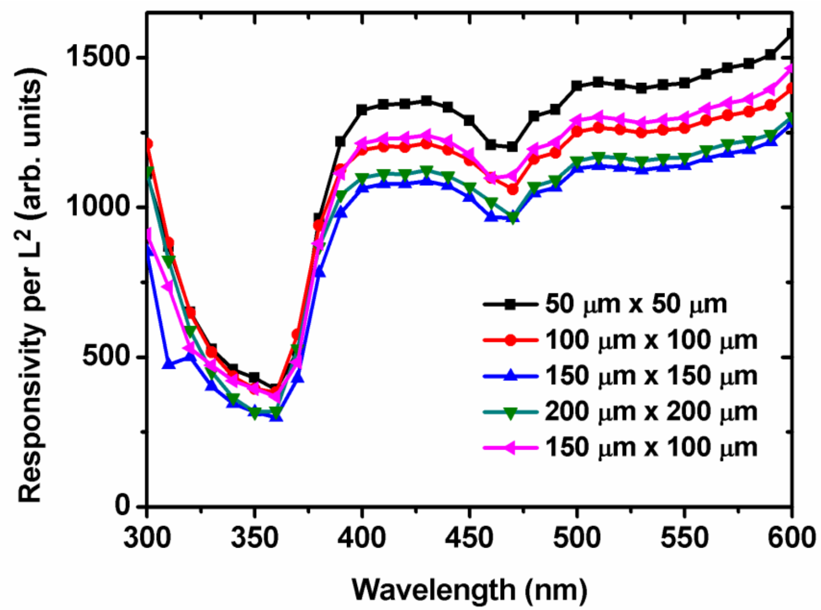

Figure 4.13: Responsivity per the square of channel length is plotted for ZnO based photo-TFTs at 250 °C. Constant V_D and V_G of -3 and 3 V are applied respectively. Legends show channel length and width respectively.

4.5 Effects of deposition temperature of channel layer on the photoresponsivity

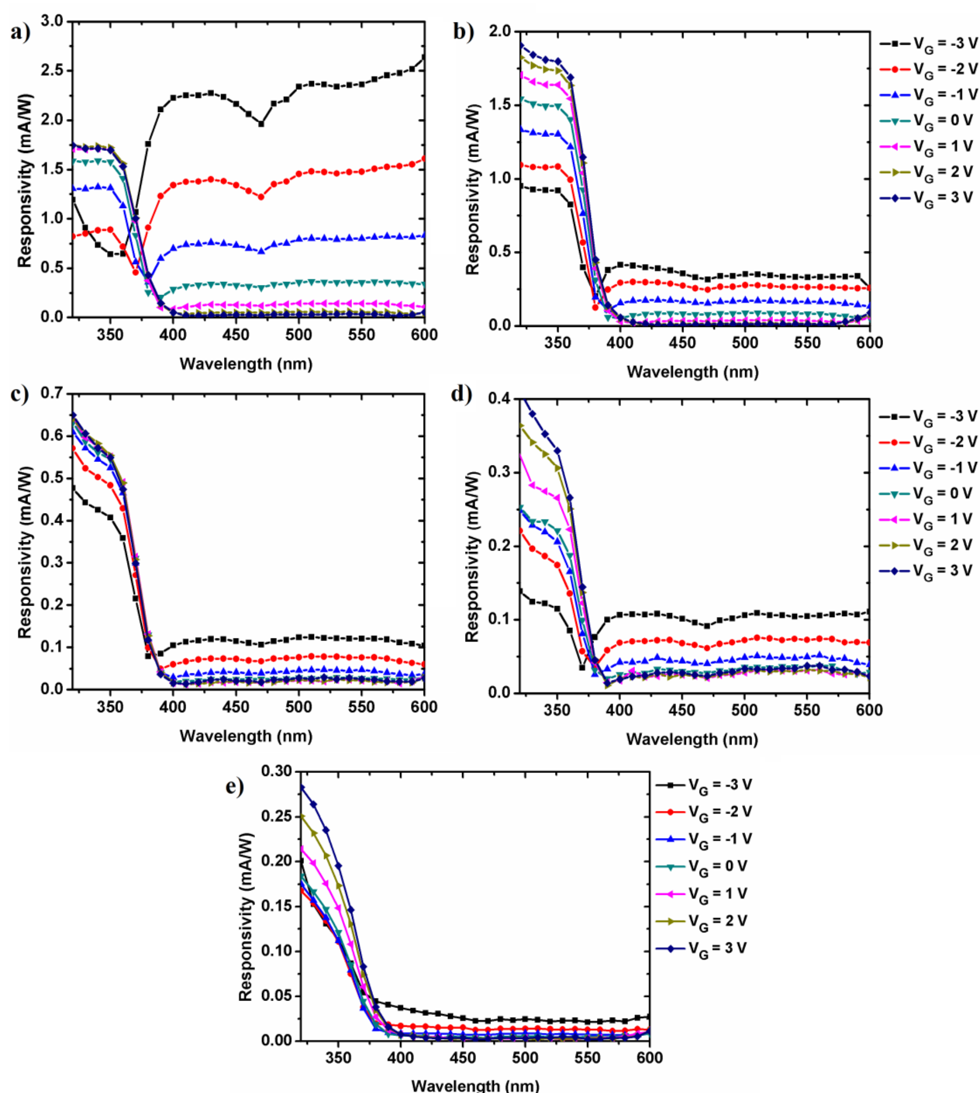

Figure 4.14: Spectral responsivity of ZnO based TFTs with a channel layer deposited at a) 250 °C, b) 200 °C, c) 120 °C, d) 100 °C, e) 80 °C. The device size is kept constant as 200 µm to 200 µm and 3 V drain bias is applied.

The devices fabricated at higher temperatures demonstrate higher photoresponse to the visible light under the same drain and gate biases (See Figure 4.14). As it is previously discussed, the subbandgap photoresponse of our devices are based on an absorption mechanism where an electron is excited from valence band to

defect states. Moreover, it is also shown that ZnO film has more defects at higher growth temperatures which could be deduced from low on/off ratio and high drain current values at these temperatures. Therefore, TFTs deposited at higher temperatures have more defects states which improve their subbandgap photoresponsivity. Furthermore, the responsivity values at λ= 550 nm is plotted separately to show the growth temperature effect more explicitly in Figure 4.15.

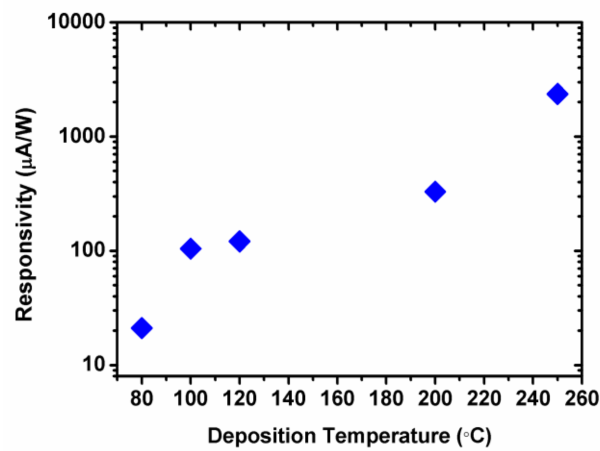

Figure 4.15: Deposition temperature dependent responsivity of ZnO based TFTs at λ = 550nm. The device size, V_G and V_D are chosen as 200 μm to 200 μm, -3 V and 3 V, respectively.

Chapter 5

Conclusions

The promising optical and electrical properties of ZnO make it a good candidate for various device applications such as UV photodetectors, LEDs, lasers and TFTs. However, it also has crystallographic defects (i.e. trap states) which is responsible from effective n-type behavior of ZnO and reduces the performances of devices based on UV light absorption or emission. In this study, a ZnO based three-terminal optoelectronic device, a photo-TFT, which benefits from these trap states is investigated.

The device structure is a combination of photoconductor and TFT. It can be described as a photoconductor with a gate terminal or a TFT with a photodetection capability, photo-TFT. This device can detect photons with energy well below ZnO's band gap through trap states and its photodetection mechanism can be actively tuned via the electric field applied from the gate terminal.

Prototype devices are fabricated in a clean room environment. The fabricated devices showed decent transistor characteristics. Especially, the devices with a channel layer deposited at 80 °C has on/off ratio of 10^9 and subthreshold slope

of 288 mV/dec. As the growth temperature of ZnO layer increases the on/off ratio and subthreshold slope performances of devices degrade. The main reason of such performance drop is the increasing number of defect states in ZnO layer at higher deposition temperatures.

Then, the optical performance of ZnO film is characterized by depositing ZnO on a double side polished quartz sample and taking absorption and photoluminescence measurements. The absorption measurements revealed that ZnO without an external control has a very low absorption in the visible region. The photoluminescence measurements demonstrated that ZnO film has a broad green emission peak which corresponds to the transition of electrons from conduction band to oxygen vacancy states.

The responsivity measurements taken from ZnO based photo-TFTs fabricated at 250 °C showed that the devices have a visible photoresponse which can be actively tuned with the gate terminal. This visible light response is due to the excitation of the valence band electrons to the unoccupied oxygen vacancy trap states. When a negative gate bias is applied, electrons inside ZnO channel are repelled and the number of unoccupied trap states increases. Therefore, the responsivity in the visible spectrum increases. On the other hand, when a positive bias is applied, electrons are attracted to the ZnO channel layer and the number of unoccupied trap states decreases. Hence, the visible light response of the device decreases. In addition to the trap related subband gap absorption mechanism, the reported devices have a photoconductive gain which improves the photocurrent value.

The effect of the device size is investigated in the photo-TFTs fabricated at 250 °C. The fabricated devices have channel width and lengths ranging from 50 μm to 200 μm. As the device size becomes smaller the responsivity of device is increased. This is explained with the $1/L^2$ dependency of the photoconductive gain term of Al/ZnO/Al structure, where L is the channel length. While the

electron is trapped in a defect state, the photogenerated hole makes multiple passes in the ZnO channel layer and for shorter-length photoconductors it makes more passes and generates more photocurrent.

The effects of the deposition temperature of ZnO channel layer on the responsivity in the visible spectrum are also investigated. The subband gap absorption mechanism of ZnO depends on the number of available (i.e. unoccupied) trap states and the number of defect states increases with the ZnO growth temperature. Therefore, exciting an electron from valence band to an unoccupied trap state at higher deposition temperatures has larger probability. Our spectral responsivity measurements also demonstrated that the responsivity of devices in the visible spectrum increases with the deposition temperature.

To summarize, in this study, it is shown that the defects of ZnO can be used for visible light photodetection, a ZnO based photoconductor can have an actively tunable visible light response with an additional gate terminal and the designed photo-TFT structure has a photoconductive gain mechanism which improves the generated photocurrent value.

The results of this thesis can be used in smart glass applications by designing an electrochromic ZnO device that has a dynamically tunable transparency with the gate terminal. Moreover, the fabricated photo-TFTs can be used as transparent visible light photodetectors by using a transparent conductive oxide as the gate metal.

In order to investigate the absorption coefficient change of ZnO films with the gate bias a metal-insulator-semiconductor-metal (MISM) structure can be used. Such structure should be formed on a quartz substrate and transparent conductive oxide layers should be used as metals. Initially, the amount of difference between transmission measurements taken under accumulated (positive) and depleted (negative) gate bias conditions can give an idea about the

absorption coefficient change of ZnO layer. To improve the difference between two bias conditions, the thickness of ZnO layer and the maximum and minimum gate bias before the gate oxide breakdown should be optimized. After selecting MISM design parameters that maximize the gate control on ZnO's absorption characteristics, ellipsometer measurements should be taken to calculate absorption coefficient (k) change of ZnO with the gate bias. It should be noted that a good absorption coefficient fit in the ellipsometer requires precise thickness information of ZnO layer and accurate refractive index data of other layers. The MISM design parameter optimization can also be done with photoluminescence measurements. By accumulating ZnO layer, the traps can be filled with electrons and the green light emission which is from the conduction band to trap state can be suppressed. On the other hand, depleting ZnO layer improves the intensity of the green emission peak by increasing the number unoccupied trap states.

Although it requires a challenging alignment stage, the same MISM structure can be illuminated from side and transmission measurements can be taken to demonstrate absorption coefficient control of ZnO layer. A detailed design for such measurement and ZnO based optical modulator structure in the visible wavelengths are already reported in our previous work [62].

Bibliography

[1] B. Cao, W. Cai, and H. Zeng, "Temperature-dependent shifts of three emission bands for ZnO nanoneedle arrays," *Appl. Phys. Lett.,* vol. 88, pp. 161101-3, 2006.

[2] C. Jagadish and S. J. Pearton, *Zinc oxide bulk, thin films and nanostructures: processing, properties, and applications*: Elsevier, 2011.

[3] D. M. Bagnall, Y. F. Chen, Z. Zhu, T. Yao, S. Koyama, M. Y. Shen, and T. Goto, "Optically pumped lasing of ZnO at room temperature," *Appl. Phys. Lett.,* vol. 70, pp. 2230-2232, 1997.

[4] P. Zu, Z. K. Tang, G. K. L. Wong, M. Kawasaki, A. Ohtomo, H. Koinuma, and Y. Segawa, "Ultraviolet spontaneous and stimulated emissions from ZnO microcrystallite thin films at room temperature," *Solid State Commun.,* vol. 103, pp. 459-463, 1997.

[5] Z. K. Tang, G. K. L. Wong, P. Yu, M. Kawasaki, A. Ohtomo, H. Koinuma, and Y. Segawa, "Room-temperature ultraviolet laser emission from self-assembled ZnO microcrystallite thin films," *Appl. Phys. Lett.,* vol. 72, pp. 3270-3272, 1998.

[6] D. K. Hwang, S. H. Kang, J. H. Lim, E. J. Yang, J. Y. Oh, J. H. Yang, and S. J. Park, "P -ZnO/ n -GaN heterostructure ZnO light-emitting diodes," *Appl. Phys. Lett.,* vol. 86, pp. 1-3, 2005.

[7] A. Tsukazaki, A. Ohtomo, T. Onuma, M. Ohtani, T. Makino, M. Sumiya, K. Ohtani, S. F. Chichibu, S. Fuke, Y. Segawa, H. Ohno, H. Koinuma, and M. Kawasaki, "Repeated temperature modulation epitaxy for p-type doping and light-emitting diode based on ZnO," *Nat. Mater.,* vol. 4, pp. 42-46, 2005.

[8] J. H. Lim, C. K. Kong, K. K. Kim, I. K. Park, D. K. Hwang, and S. J. Park, "UV electroluminescence emission from ZnO light-emitting diodes grown by high-temperature radiofrequency sputtering," *Adv. Mater.,* vol. 18, pp. 2720-2724, 2006.

[9] Y. Ryu, T. S. Lee, J. A. Lubguban, H. W. White, B. J. Kim, Y. S. Park, and C. J. Youn, "Next generation of oxide photonic devices: ZnO-based ultraviolet light emitting diodes," *Appl. Phys. Lett.,* vol. 88, 2006.

[10] M. H. Huang, S. Mao, H. Feick, H. Yan, Y. Wu, H. Kind, E. Weber, R. Russo, and P. Yang, "Room-Temperature Ultraviolet Nanowire Nanolasers," *Science,* vol. 292, pp. 1897-1899, June 8, 2001 2001.

[11] J. F. Wager, "Transparent Electronics," *Science,* vol. 300, pp. 1245-1246, May 23, 2003 2003.

[12] E. Fortunato, P. Barquinha, and R. Martins, "Oxide Semiconductor Thin-Film Transistors: A Review of Recent Advances," *Adv. Mater.,* vol. 24, pp. 2945-2986, 2012.

[13] S. Masuda, K. Kitamura, Y. Okumura, S. Miyatake, H. Tabata, and T. Kawai, "Transparent thin film transistors using ZnO as an active channel layer and their electrical properties," *J. Appl. Phys.,* vol. 93, pp. 1624-1630, 2003.

[14] R. L. Hoffman, B. J. Norris, and J. F. Wager, "ZnO-based transparent thin-film transistors," *Appl. Phys. Lett.,* vol. 82, pp. 733-735, 2003.

[15] P. F. Carcia, R. S. McLean, M. H. Reilly, and G. Nunes, "Transparent ZnO thin-film transistor fabricated by rf magnetron sputtering," *Appl. Phys. Lett.,* vol. 82, pp. 1117-1119, 2003.

[16] J. Zhu, H. Chen, G. Saraf, Z. Duan, Y. Lu, and S. T. Hsu, "ZnO TFT Devices Built on Glass Substrates," *J. Elec. Materi,* vol. 37, pp. 1237-1240, 2008/09/01 2008.

[17] S.-H. K. Park, C.-S. Hwang, M. Ryu, S. Yang, C. Byun, J. Shin, J.-I. Lee, K. Lee, M. S. Oh, and S. Im, "Transparent and Photo-stable ZnO Thin-film Transistors to Drive an Active Matrix Organic-Light-Emitting-Diode Display Panel," *Adv. Mater.,* vol. 21, pp. 678-682, 2009.

[18] K. M. Choi, G. W. Hyung, J. W. Yang, J. R. Koo, Y. K. Kim, S. J. Kwon, and E. S. Cho, "Fabrication of Atomic Layer Deposited Zinc Oxide Thin Film Transistors with Organic Gate Insulator on Flexible Substrate," *Mol. Cryst. Liq. Cryst.,* vol. 529, pp. 131-136, 2010/10/08 2010.

[19] K. Nomura, H. Ohta, A. Takagi, T. Kamiya, M. Hirano, and H. Hosono, "Room-temperature fabrication of transparent flexible thin-film transistors using amorphous oxide semiconductors," *Nature,* vol. 432, pp. 488-492, 2004.

[20] P. Görrn, M. Sander, J. Meyer, M. Kröger, E. Becker, H. H. Johannes, W. Kowalsky, and T. Riedl, "Towards See-Through Displays: Fully

Transparent Thin-Film Transistors Driving Transparent Organic Light-Emitting Diodes," *Adv. Mater.,* vol. 18, pp. 738-741, 2006.

[21] K. Jang-Yeon, S. Kyoung-Seok, J. Ji Sim, K. Tae Sang, R. Myung Kwan, P. Kyung-Bae, Y. Byung Wook, K. Jung Woo, Y. G. Lee, P. Kee Chan, L. Sang-Yoon, and K. Jong-Min, "Bottom-Gate Gallium Indium Zinc Oxide Thin-Film Transistor Array for High-Resolution AMOLED Display," *IEEE Electron Devic. Lett.,* vol. 29, pp. 1309-1311, 2008.

[22] T. Hirao, M. Furuta, T. Hiramatsu, T. Matsuda, L. Chaoyang, H. Furuta, H. Hokari, M. Yoshida, H. Ishii, and M. Kakegawa, "Bottom-Gate Zinc Oxide Thin-Film Transistors (ZnO TFTs) for AM-LCDs,", *IEEE T. Electron Dev.,* vol. 55, pp. 3136-3142, 2008.

[23] D. Loy, "Challenges in Flexible Electronics Technology," Flexible Display Center at ASU2011.

[24] U. Ozgur, Y. I. Alivov, C. Liu, A. Teke, M. A. Reshchikov, S. Dogan, V. Avrutin, S. J. Cho, and H. Morkoc, "A comprehensive review of ZnO materials and devices," *J. Appl. Phys.,* vol. 98, pp. 041301-103, 2005.

[25] Y. Liu, C. R. Gorla, S. Liang, N. Emanetoglu, Y. Lu, H. Shen, and M. Wraback, "Ultraviolet detectors based on epitaxial ZnO films grown by MOCVD," *J. Elec. Mater.,* vol. 29, pp. 69-74, 2000/01/01 2000.

[26] S. Liang, H. Sheng, Y. Liu, Z. Huo, Y. Lu, and H. Shen, "ZnO Schottky ultraviolet photodetectors," *J. Cryst. Growth,* vol. 225, pp. 110-113, 2001.

[27] D. C. Oh, T. Suzuki, T. Hanada, T. Yao, H. Makino, and H. J. Ko, "Photoresponsivity of ZnO Schottky barrier diodes,", *J. Vac. Sci. Technol.*, 2006, pp. 1595-1598.

[28] X. G. Zheng, Q. S. Li, J. P. Zhao, D. Chen, B. Zhao, Y. J. Yang, and L. C. Zhang, "Photoconductive ultraviolet detectors based on ZnO films," *Appl. Surf. Sci.,* vol. 253, pp. 2264-2267, 2006.

[29] K. W. Liu, J. G. Ma, J. Y. Zhang, Y. M. Lu, D. Y. Jiang, B. H. Li, D. X. Zhao, Z. Z. Zhang, B. Yao, and D. Z. Shen, "Ultraviolet photoconductive detector with high visible rejection and fast photoresponse based on ZnO thin film," *Solid State Electron.,* vol. 51, pp. 757-761, 2007.

[30] D. C. Look and B. Claflin, "P-type doping and devices based on ZnO," *Phys. Stat. Solid. B.,* vol. 241, pp. 624-630, 2004.

[31] Y. R. Ryu, T. S. Lee, J. H. Leem, and H. W. White, "Fabrication of homostructural ZnO p--n junctions and ohmic contacts to arsenic-doped p-type ZnO," *Appl. Phys. Lett.,* vol. 83, pp. 4032-4034, 2003.

[32] K.-K. Kim, H.-S. Kim, D.-K. Hwang, J.-H. Lim, and S.-J. Park, "Realization of p-type ZnO thin films via phosphorus doping and thermal activation of the dopant," *Appl. Phys. Lett.,* vol. 83, pp. 63-65, 2003.

[33] D. C. Look, D. C. Reynolds, C. W. Litton, R. L. Jones, D. B. Eason, and G. Cantwell, "Characterization of homoepitaxial p-type ZnO grown by molecular beam epitaxy," *Appl. Phys. Lett.,* vol. 81, pp. 1830-1832, 2002.

[34] Y. R. Ryu, S. Zhu, D. C. Look, J. M. Wrobel, H. M. Jeong, and H. W. White, "Synthesis of p-type ZnO films," *J. Cryst. Growth,* vol. 216, pp. 330-334, 2000.

[35] T. Aoki, Y. Hatanaka, and D. C. Look, "ZnO diode fabricated by excimer-laser doping," *Appl. Phys. Lett.,* vol. 76, pp. 3257-3258, 2000.

[36] H. Kind, H. Yan, B. Messer, M. Law, and P. Yang, "Nanowire Ultraviolet Photodetectors and Optical Switches," *Adv. Mater.,* vol. 14, pp. 158-160, 2002.

[37] C. Soci, A. Zhang, B. Xiang, S. A. Dayeh, D. P. R. Aplin, J. Park, X. Y. Bao, Y. H. Lo, and D. Wang, "ZnO Nanowire UV Photodetectors with High Internal Gain," *Nano Letters,* vol. 7, pp. 1003-1009, 2007/04/01 2007.

[38] K. J. Chen, F. Y. Hung, S. J. Chang, and S. J. Young, "Optoelectronic characteristics of UV photodetector based on ZnO nanowire thin films," *J. Alloy Compd.,* vol. 479, pp. 674-677, 2009.

[39] S. Vempati, J. Mitra, and P. Dawson, "One-step synthesis of ZnO nanosheets: a blue-white fluorophore," *Nanoscale Res. Lett.,* vol. 7, p. 470, 2012.

[40] C. H. Ahn, Y. Y. Kim, D. C. Kim, S. K. Mohanta, and H. K. Cho, "A comparative analysis of deep level emission in ZnO layers deposited by various methods," *J. Appl. Phys.,* vol. 105, pp. 013502-5, 2009.

[41] S. Jeon, S.-E. Ahn, I. Song, C. J. Kim, U. I. Chung, E. Lee, I. Yoo, A. Nathan, S. Lee, J. Robertson, and K. Kim, "Gated three-terminal device architecture to eliminate persistent photoconductivity in oxide

semiconductor photosensor arrays," *Nat. Mater.,* vol. 11, pp. 301-305, 2012.

[42] Y. P. Varshni, "Temperature dependence of the energy gap in semiconductors," *Physica,* vol. 34, pp. 149-154, 1967.

[43] F. B. Oruc, L. E. Aygun, I. Donmez, H. Y. Yu, N. Biyikli, and A. K. Okyay, "Investigation of Electrical and Optical Properties of Atomic Layer Deposited ZnO Thin Film Transistors," *in preparation*.

[44] H. Morkoç and Ü. Özgür, "Optical Properties," in *Zinc Oxide*, ed: Wiley-VCH Verlag GmbH & Co. KGaA, 2009, pp. 131-244.

[45] B. Cao, W. Cai, Y. Li, F. Sun, and L. Zhang, "Ultraviolet-light-emitting ZnO nanosheets prepared by a chemical bath deposition method," *Nanotechnology,* vol. 16, p. 1734, 2005.

[46] S. J. Chen, Y. C. Liu, C. L. Shao, R. Mu, Y. M. Lu, J. Y. Zhang, D. Z. Shen, and X. W. Fan, "Structural and Optical Properties of Uniform ZnO Nanosheets," *Adv. Mater.,* vol. 17, pp. 586-590, 2005.

[47] E. Przeździecka, W. Ł, W. Paszkowicz, E. Łusakowska, T. Krajewski, G. Łuka, E. Guziewicz, and M. Godlewski, "Photoluminescence, electrical and structural properties of ZnO films, grown by ALD at low temperature," *Semiconductor Sci. Tech.,* vol. 24, p. 105014, 2009.

[48] H. Zeng, Z. Li, W. Cai, and P. Liu, "Strong localization effect in temperature dependence of violet-blue emission from ZnO nanoshells," *J. Appl. Phys.,* vol. 102, pp. 104307-4, 2007.

[49] B. Lin, Z. Fu, and Y. Jia, "Green luminescent center in undoped zinc oxide films deposited on silicon substrates," *Appl. Phys. Lett.,* vol. 79, pp. 943-945, 2001.

[50] P. S. Xu, Y. M. Sun, C. S. Shi, F. Q. Xu, and H. B. Pan, "The electronic structure and spectral properties of ZnO and its defects," *Nuclear Instrum. Met. Phys. Res. B,* vol. 199, pp. 286-290, 2003.

[51] S. B. Zhang, S. H. Wei, and A. Zunger, "Intrinsic n-type versus p-type doping asymmetry and the defect physics of ZnO," *Phys. Rev. B,* vol. 63, p. 075205, 2001.

[52] X. L. Wu, G. G. Siu, C. L. Fu, and H. C. Ong, "Photoluminescence and cathodoluminescence studies of stoichiometric and oxygen-deficient ZnO films," *Appl. Phys. Lett.,* vol. 78, pp. 2285-2287, 2001.

[53] D. Li, Y. H. Leung, A. B. Djurisic, Z. T. Liu, M. H. Xie, S. L. Shi, S. J. Xu, and W. K. Chan, "Different origins of visible luminescence in ZnO nanostructures fabricated by the chemical and evaporation methods," *Appl. Phys. Lett.,* vol. 85, pp. 1601-1603, 2004.

[54] H. Asakura and M. Iida, "Diffraction grating unit and second-harmonic generator employing the same," ed: Google Patents, 1995.

[55] E. G. Loewen and E. Popov, *Diffraction gratings and applications*: CRC Press, 1997.

[56] E. Loewen and C. Palmer, *Diffraction grating handbook*: Newport Corporation, 2005.

[57] A. Ortiz-Conde, F. J. García Sánchez, J. J. Liou, A. Cerdeira, M. Estrada, and Y. Yue, "A review of recent MOSFET threshold voltage extraction methods," *Microelectron. Reliab.,* vol. 42, pp. 583-596, 2002.

[58] E. Fortunato, A. Pimentel, L. Pereira, A. Gonçalves, G. Lavareda, H. Águas, I. Ferreira, C. N. Carvalho, and R. Martins, "High field-effect mobility zinc oxide thin film transistors produced at room temperature," *J. Non-Cryst. Sol.,* vol. 338–340, pp. 806-809, 2004.

[59] S. Kwon, S. Bang, S. Lee, S. Jeon, W. Jeong, H. Kim, S. C. Gong, H. J. Chang, H.-h. Park, and H. Jeon, "Characteristics of the ZnO thin film transistor by atomic layer deposition at various temperatures," *Semiconductor Sci. Tech.,* vol. 24, p. 035015, 2009.

[60] J. Siddiqui, E. Cagin, D. Chen, and J. D. Phillips, "ZnO thin-film transistors with polycrystalline (Ba,Sr)TiO_3 gate insulators," *Appl. Phys. Lett.,* vol. 88, pp. 212903-212903-3, 2006.

[61] N. Huby, S. Ferrari, E. Guziewicz, M. Godlewski, and V. Osinniy, "Electrical behavior of zinc oxide layers grown by low temperature atomic layer deposition," *Appl. Phys. Lett.,* vol. 92, pp. 023502-023502-3, 2008.

[62] A. K. Okyay, L. E. Aygün, and F. B. Oruç, "ZnO based optical modulator in the visible wavelengths," *Proc. SPIE* 2013, pp. 86261T-86261T-6.